International Journal of Concrete Structures and Materials

RESEARCH

Open Access

Application of Artificial Neural Network for Prediction of Concrete–High-Performance Concrete Interfacial Bond Strength After Exposure to Elevated Temperature

Nagat M. Zalhaf[1*]

Abstract

High-performance concrete (HPC) is a new advanced building material for highway bridges, building construction, and repair/strengthen concrete structures with fire risk owing to its high fire resistance. The concrete composites should have interfacial bond strength (IBS) that is sufficient to transfer load between concrete components. When those composite structures are exposed to fire, horizontal cracks have been observed, and in some cases, the concrete layers have separated depending on the fire intensity. Therefore, the assessment of the IBS between the two concrete layers after exposure to fire is important for examining the entire fire behavior. Thus, the purpose of this work is to create an artificial neural network (ANN) model between statistically important factors and the IBS after exposure to elevated temperatures for using in the structural fire design of composite concrete layers. A total of 467 data points, including 252 data points from the slant shear test, 87 data points from the push-off test, and 128 data points from the tensile test, have been collected from literature reviews. Firstly, the independent parameters such as interfacial surface roughness, temperature exposure, part of the specimen exposed to temperature, type of concrete overlay, and fiber content introduced in the concrete overlay were carefully analyzed to identify the statistically important parameters and their impact on the IBS. Secondly, a designed ANN model has been developed to predict the IBS based on the type of test technique, interfacial surface roughness, temperature exposure, type of concrete overlay, and fiber content. Moreover, a mathematical model has been proposed to predict the IBS between concrete substrate and HPC after exposure to elevated temperature. Finally, the predicted IBS from the design ANN model and the mathematical IBS were compared with the available empirical models from literature. The outcome results demonstrated that the design ANN model was able to predict the IBS between two concrete layers after exposure to elevated temperatures with a coefficient of determination R^2 of 0.97, while the mathematical IBS gave a good accuracy for predicting the IBS in the case of the interface under combined stress with R^2 equal to 0.90. This study effectively bridges the gaps in both theoretical and experimental findings by integrating ANN models with advanced computational techniques and robust statistical analyses. This multifaceted approach not only enriches our understanding of the topic, but also provides more precise insights and predictive capabilities.

Keywords Prediction, Interface bond strength, An artificial neural network, Elevated temperatures

Journal information: ISSN 1976-0485 / eISSN 2234-1315.

*Correspondence:
Nagat M. Zalhaf
nagat.zalhaf@eng.kfs.edu.eg
[1] Department of Civil Engineering, Faculty of Engineering, Kafrelsheikh University, Kafr El-Shaikh 33511, Egypt

1 Introduction

Fire exposure is considered one of the worst risks that reinforced concrete (RC) structures could face during their service life. The load-bearing capacity of the RC

structure exposed to fire was reduced due to the deterioration of mechanical properties for concrete and reinforcing steel (Gao et al., 2018). These RC structures need to be repaired and strengthened to improve their capacity. Rehabilitation by adding a new concrete layer to the concrete substrate is one of the most common repair methods (Santos & Julio, 2007). High-performance concrete has achieved advances as a repair or strengthening material for concrete structures due to its improved mechanical properties, which include high strength, durability, ductility, and higher fire resistance (Ghazy et al., 2023).

The interfacial surface between the new and old concrete is considered the weakest part of the composite concrete structure (Chen et al., 2023). To evaluate concrete–concrete interfacial bond strength (IBS), a number of test techniques have been developed depending on the type of applied load to the interface (Daneshvar et al., 2022). There are three main categories of test methods, such as tensile, shear, and mixed-mode tests, as presented in Fig. 1. Momayez et al. (2005) concluded that the IBS can be varied by a factor of 8 depending on the type of test technique. Furthermore, the failure modes of the composite concretes depend on the type of applying load and concrete overlay types used (Gao et al., 2018).

The interfacial bond strength (IBS) between two concrete layers displayed more deterioration at elevated temperature than the deterioration in the concrete mechanical properties (Chen et al., 2023). This is due to many reasons including evaporation of the free water and water in hydration gel matrix at temperature of 100 °C (Babalola et al., 2021), resulting in more voids in the concrete which weaken concrete structure and consequently loss in the IBS. The decomposition of calcium silicate hydrate gel at temperature higher than 400 °C, the disintegration of aggregate at temperature above 600 °C, all of these led to more degradation in the chemical bond and mechanical bit forces (Cao et al., 2023). In addition,

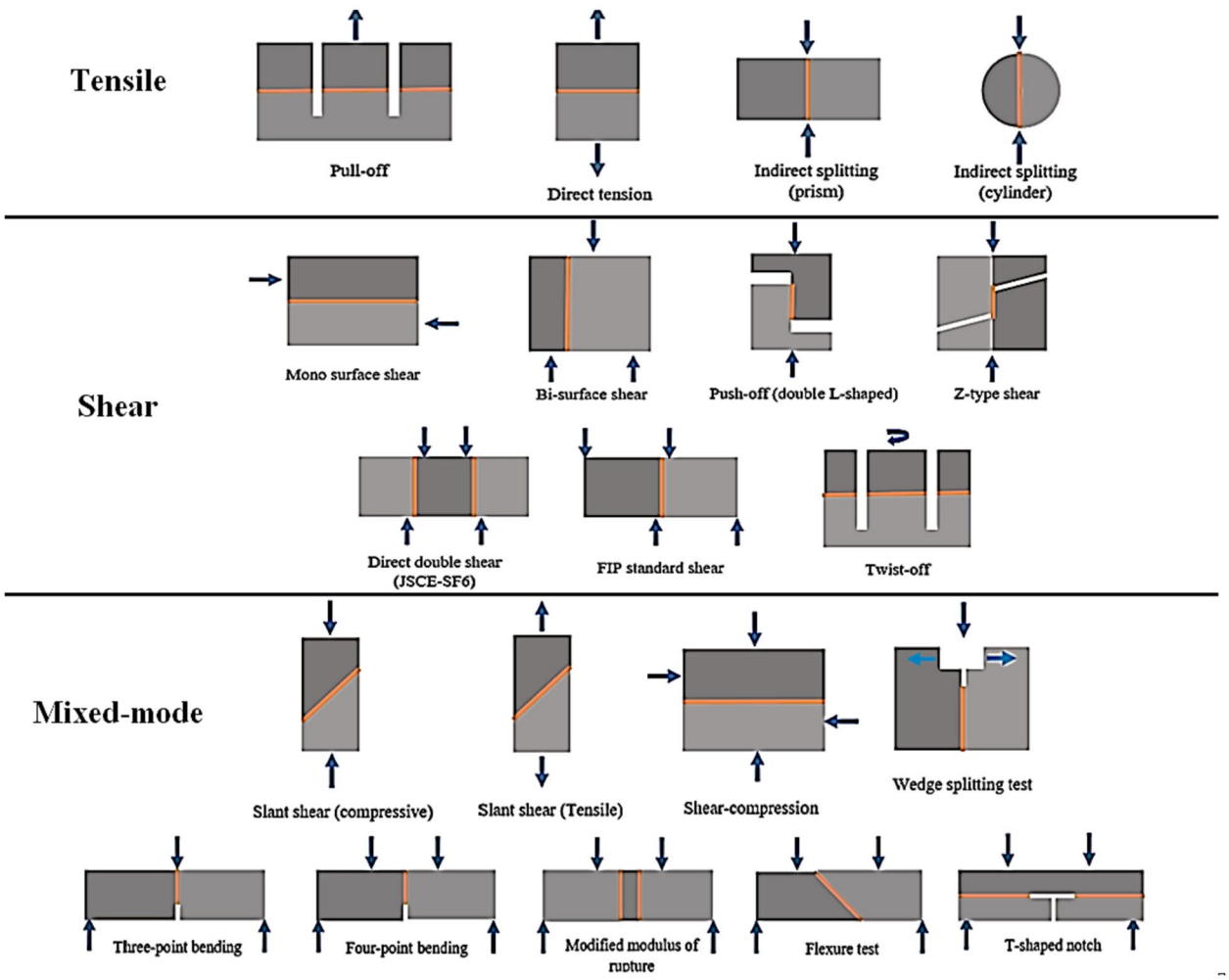

Fig. 1 Illustration of the several test techniques used to measure the strength of the concrete-to-concrete connection (Daneshvar et al., 2022)

the thermal incompatibility between cement matrix and aggregate in one hand and between the different concrete types in the other hand, which create micro-crack at the interface between the two concrete layers and, consequently the reduction in the IBS (Ma et al., 2015; Zalhaf et al., 2024).

Many studies have been conducted to improve the IBS after exposure to elevated temperatures and concluded that the interfacial bond is mainly affected by many factors, including interfacial surface roughness (Abo Sabah et al., 2019; Behforouz et al., 2023; Chen et al., 2023; Haido et al., 2021), concrete overlay strength (Zalhaf et al., 2024), bonding agent (Gao et al., 2019; Shang et al., 2021), inclusion of fiber (Abo Sabah et al., 2019; Gao et al., 2019; Haido et al., 2021; Zalhaf et al., 2024), as shown in Fig. 2, and interfacial moisture condition (Shang et al., 2021). Furthermore, in direct shear and tensile tests, the degradation in IBS was more obvious in the case of smooth surfaces than in the case of rough surfaces, as depicted in Fig. 3, while the slant shear test recorded the least degradation in the interfacial bond strength (Chen et al., 2023).

Several researchers developed a mathematical model to predict the IBS between two concrete layers at room temperature (Gohnert, 2003; Randl, 1997; Santos & Julio, 2010). In addition, the standards codes gave design expression for the IBS between the old concrete and the strengthened materials, where the main parameters are the interface roughness and reinforcement across the interface (ACI 318, 2008; CEB-FIP, 1990; Eurocode 2, 2004).

At elevated temperatures, very limited models have been proposed to predict the IBS between two concrete layers after exposure to elevated temperatures. Guo et al. (2004) developed an empirical equation to predict the interfacial strength between an old concrete and a new concrete layer after exposure to high temperatures. The results showed that the IBS was influenced by elevated temperature, interfacial surface roughness, and the compressive strength of a weak concrete layer, as depicted in Eqs. 1–3:

$$\mathrm{IS} = \lambda F_c, \tag{1}$$

$$\lambda = 0.048\beta - \alpha_1 T^2 + (\gamma - \alpha_2 T)\omega, \tag{2}$$

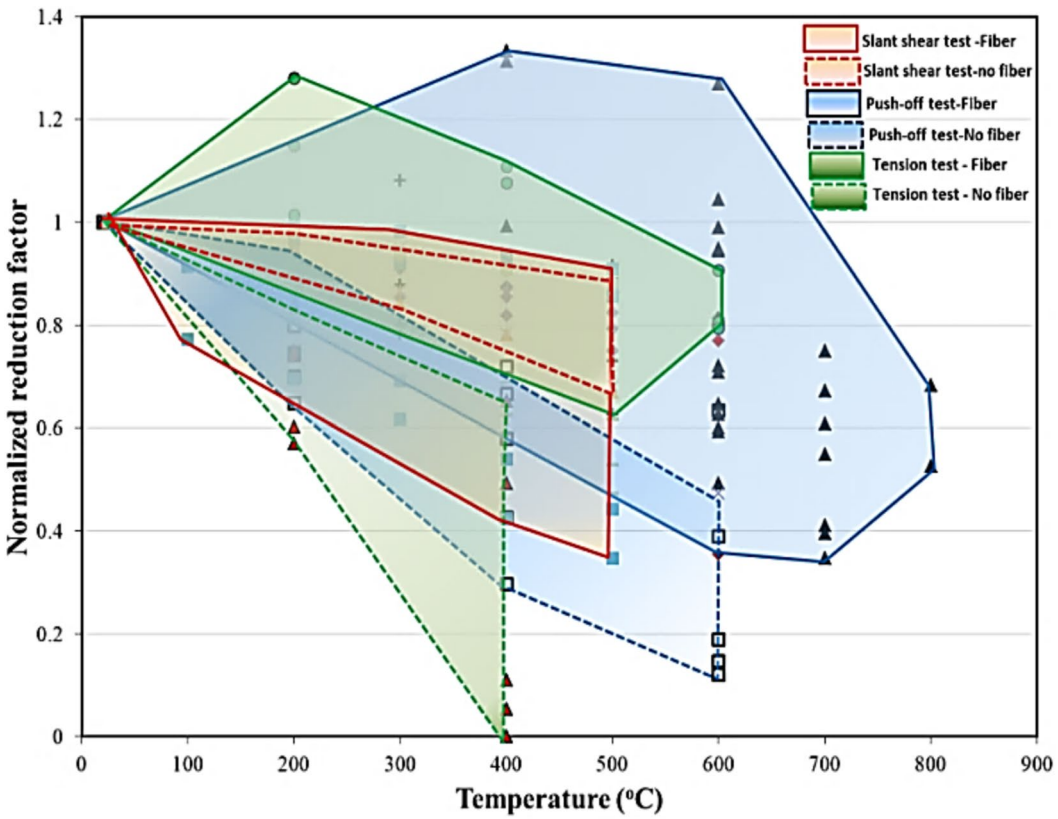

Fig. 2 Effect of fiber on the IBS for different tests, dataset obtained from Zalhaf et al. (2024), Abo Sabah et al. (2019), Haido et al. (2021), Gao et al. (2019)

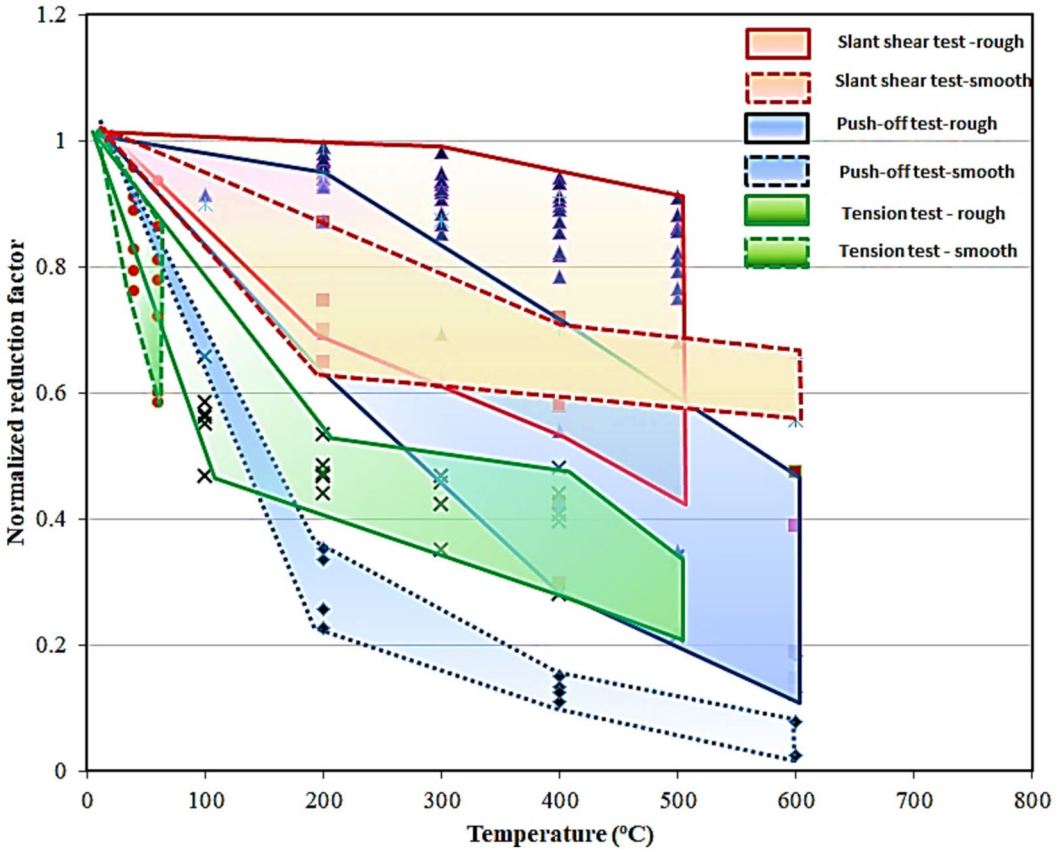

Fig. 3 Effect of interfacial surface roughness on the IBS, dataset obtained from Chen et al. (2023), Behforouz et al. (2023), Gao et al. (2019)

$$\omega = \begin{cases} h, & h \le 1.5 \\ 1.5 & h < 1.5 \end{cases}, \tag{3}$$

where $\alpha_1 = 1.9248 \times 10^{-8}$, $\alpha_2 = 2.2825 \times 10^{-5}$, $\gamma = 0.0279$, β is a factor dependent on interface agent and equals 1, 1.15, 1.05 for no interface agent, cement slurry was used, cement swelling slurry, respectively, and f_c is the compressive strength of concrete substrate.

Chen et al. (2023) concluded that the IBS depended on the interfacial surface roughness and elevated temperature and proposed a mathematical model to quantify the effect of the two parameters in the IBS as presented in Eqs. 4–5:

$$\mathrm{IBS}_T = \eta \mathrm{IBS}_{20} \text{ for smooth surface}, \tag{4}$$

$$\eta = e^{-A(T-20)} \text{ for rough surface}, \tag{5}$$

where η is the coefficient of degradation in the interfacial bond strength, IBS_T is the interfacial strength at elevated temperature, IBS_{20} is the interfacial strength at room temperature, A is the coefficient of degradation factor of the interface roughness and taken as 0.001 and 0.003 for upper and lower limit, respectively.

Shang et al. (2021) used the coefficient of cohesion to develop a mathematical model for predicting IBS between normal-strength concrete NSC substrate and engineering cementitious composite. They found that the coefficient of cohesion is influenced by the surface roughness and temperature exposure as depicted in Eqs. 6–8:

$$\mathrm{IBS}(T,R) = c_T c_R f_c, \tag{6}$$

$$\begin{cases} c_T = 1.478 \times 10^{-4} T + 0.04819 & \text{for } 0 \le T \le 400C \\ c_T = 1.783 \times 10^{-4} T + 0.1814 & \text{for } 400 \le T \le 700C \end{cases} \tag{7}$$

$$\begin{cases} c_R = 0.381R + 0.0134 & \text{for } 1.5 \text{ mm} \le R \le 3.5 \text{ mm} \\ c_R = -1.151R + 5.547 & \text{for } 3.5 \text{ mm} \le R \le 4.5 \text{ mm} \end{cases} \tag{8}$$

where T is the temperature exposure, R is the surface roughness, c_T and c_R are the coefficient of adhesion corresponding T and R, respectively.

Soft computing programs, such as gene expression programming and artificial intelligence (AI) have caught the attention of civil engineering researchers in the last few years (Abbas et al., 2019; Al Hamd et al., 2022; Albostami et al., 2023; Farhangi et al., 2024; Yehia et al., 2024). The artificial neural network is a type of AI that is based on the identification of the relationship between independent input and dependent output parameters through the use of training methods (Elsanadedy et al., 2012, 2014, 2016). In cases of elevated temperatures, several ANN models have been developed, such as predicting the mechanical properties of concrete materials after exposure to elevated temperatures (Abbas et al., 2019; Chen et al., 2021; Farhangi et al., 2024; Shafighfard et al., 2022), predicting the temperature distribution in RC slabs (Ghazy et al., 2021), and predicting the fire resistance of RC beams strengthened with fiber-reinforced polymers (Naser et al., 2012).

1.1 Significance of the Research

As discussed above, the IBS after exposure to elevated temperatures is not only affected by the temperature exposure, but there are many parameters that significantly affect it. The existing code standards anticipated that the IBS would only be based on cohesion and friction coefficients, which did not account for temperature effects or other influencing factors. Moreover, these codes are based on the bond strength between NSC and NSC data and neglect the effect of concrete overlay type and fiber, which may give inaccurate results for NSC–HPC interfacial bond strength. In addition, a few studies have empirical equations for predicting the IBS after exposure to elevated temperatures. However, the majority of these current models either focus on the compressive strength of the concrete substrate, temperature exposure, or interface surface properties. For application in structural fire design, this work attempts to establish predictive correlations between the most influential parameters and the ensuing loss in the IBS between the two concrete layers. Therefore, the significance of this research is to demonstrate the usefulness of the ANN model in solving challenging issues like fire-induced degradation of the IBS between two concrete layers. Moreover, an extensive study has been conducted to assess the effect of different parameters on the interfacial bond strength, including interfacial roughness, temperature exposure, part of the specimen exposed to temperature, type of concrete overlay, and fiber content introduced in the concrete overlay. Finally, a mathematical model was developed to predict the IBS at different temperatures, including the significant parameters obtained from the ANN model. This advancement could improve the predictive ability of structural engineering processes by lowering the need for costly experimental testing during construction.

2 Data Base

An artificial neural network model was used to study the correlation between independent (input) and dependent (output) variables. To create the data base, an extensive review was carried out. A total of 467 data points were collected from previous studies (Abo Sabah et al., 2019; Albidah et al., 2020; Behforouz et al., 2023; Chen et al., 2023; Gao et al., 2019; Haido et al., 2021; Ouyang et al., 2023; Shang et al., 2021; Sun et al., 2022; Zalhaf et al., 2024). Three data sets were used in this study include the slant shear test (252 data points), the push-off test (87 data points), and the tensile test (128 data points). From the comprehensive review of previous studies listed in Table 1, it can be concluded that the IBS at elevated temperatures is more sensitive to many parameters, such as concrete substrate surface preparation technique, elevated temperature, type of concrete overlay, inclusion of fiber in the concrete overlay, part of the specimen exposed to temperature, and shear angle in the case of a slant shear test.

This database was used to construct three ANN models based on the technique used in conducting the test. Model I consists of a data set from a slant shear test, where the model studied the correlation between the independent variables, which include; temperature degree, fiber content, the part of the specimen exposed to temperature (HP), type of concrete overlay (CO), concrete substrate surface preparation technique (surface roughness type, SR), and shear angle (α). According to the part of the specimen exposed to elevated temperatures, there are two categories. The first is that the concrete substrate is strengthened with a concrete overlay and then exposed to an elevated temperature (composite specimen). The second is that the concrete substrate is exposed to elevated temperatures, then repaired with a concrete overlay (concrete substrate). Two types of concrete overlay are used (NSC and HPC). Concrete substrate surface treatment plays an important role in the interfacial bond strength. Thus, the surface of the concrete substrate perpetration method is classified into six (6) categories such as smooth surfaces (S), sandblast surfaces (SB), wire brushes (WB), holes (H), grooves (G), and combined interface roughness (C). The output-dependent variable was the interfacial bond strength (IBS).

In ANN models II and III, the input independent variables are the same as those included in model I except for the shear angle, while the output parameter is the interfacial bond strengths obtained from the tensile test and push-off test for ANN II and ANN III, respectively. The

Table 1 The main finding in previous studies on the IBS between concrete substrate and concrete overlay at elevated temperature

References	Parameters	Outcome
Abo Sabah et al. (2019)	Type of surface roughness, temperature	Temperature had an adverse effect on IBS The type of surface roughness had a significant effect on the IBS, where the best enhancement was obtained with SB at elevated temperature
Haido et al. (2021)	Fiber content, temperature, type of surface roughness	Increased fiber content of concrete overlay led to improved IBS SB method achieved the highest IBS
Behforouz et al. (2023)	Temperature, type of surface roughness	The IBS between NSC and HPC overlay substantially depends on temperature exposure, surface roughness type, and type of concrete overlay. Increased fly ash concrete achieved an improvement in the IBS by 71%
Gao et al. (2019)	Temperature, part exposed to temperature, type of concrete overlay	Concrete overlay affected significantly on the IBS, where using HPC can enhance the IBS, especially in the case of the composite specimen exposed to fire Using NSC as a strengthening material showed serious burst at elevated temperature
Sun et al. (2022)	Temperature, shear angle	Temperature affect adversely on the IBS, where the cracks are obviously appear at the interface at temperature higher than 300 °C Shear angle of 30 38 45 displayed IBS of 146, 137 and 110% at temperature of 200 °C as compared to 100 °C, while at 700 °C increase shear angle showed an increase in IBS
Chen et al. (2023)	Type of concrete overlay, temperature, type of surface roughness	However, using high-strength concrete as repair material notably enhances the IBS; it showed a progressive deterioration after exposure to elevated temperatures Surface roughness and elevated temperature are the main parameters affected in the IBS
Zalhaf et al. (2024)	Temperature, type of concrete overlay, fiber content	Concrete overlay plays an important role in the IBS after exposure to elevated temperatures. At temperature of 800 °C, the specimen showed explosive spalling. Using fiber can improve the IBS at elevated temperatures.
Shang et al. (2021)	Temperature, type of concrete overlay, type of surface roughness	Temperature blow 400 °C, the IBS increased with increasing temperature, while above this temperature the IBS displayed decreased rapidly. Increased degree of surface roughness above 3.5 mm led to a decrease the IBS
Gao et al. (2019)	Type of surface roughness, concrete overlay, temperature	The IBS increases with increasing degree of surface roughness and compressive strength of the concrete overlay, while decreasing with temperature increase
Ouyang et al. (2023)	Temperature	Temperature exposure increased the porosity at the interface and caused a decrease in the IBS

data bases for the deferent three models are summarized in Appendix part.

Table 2 presents the statistical analysis of the input and output numerical parameters, while the categorical parameters are represented as a pie chart as shown in Fig. 4. The marginal plots and normal distribution for parameters in binary combinations for push-off, slant shear, and tensile testing are displayed in Fig. 5. The statistical calculations include mean, standard deviation, variance, skewness, kurtosis, quartiles, and normality test. Skewness and kurtosis are used for describing the shape of the probability distribution, where kurtosis refers to the flatness of the distribution and skewness is used to indicate the symmetry of data around the mean. The value of kurtosis near zero means the shape is close to normal, while the zero value of skewness indicates the distribution is symmetric. When the skewness value is greater than 1, it shows that the data are significantly skewed. A positive skew implies that the data have a lengthy tail in the positive direction (Abbas et al., 2019). The conclusions drawn from the marginal plots and statistical analysis are:

1. According normality test, the *P*-value (at 0.05 significance level) is less than 0.005 for all parameters which mean that reject normality and the distribution is not normal. The higher value of *A*-squared verifies that the distribution of the data is not normal.
2. The surface roughness type had a significant effect on the IBS for different types of tests (slant shear, push-off, and tensile tests), as shown in Fig. 5a. It can be established from the figure that the IBS notably

Table 2 Statistics input numerical parameters for different tests

Statistical parameter	Direct shear test 87 data point			Tension test 128 data point			Slant shear test 252 data point				
	Temperature	Fiber	Interfacial strength	Temperature	Fiber	Interfacial strength	Interfacial	Temperature	Fiber	Angle	Interfacial strength
Mean	397.99	0.874	1.889	288.7	2.32	1.90		318.2	0.63	30.48	12.92
Std. deviation	250.343	0.956	1.082	203.7	2.25	1.23		219.1	1.33	1.89	10.28
Variance	62,671.7	0.914	1.172	41,399	5.08	1.52		48,007	1.78	3.59	105.8
Skewness	− 0.339	0.279	0.289	0.397	0.458	2.35		0.254	3.14	3.75	0.41
Kurtosis	− 1.376	− 1.88	0.373	− 0.474	− 1.45	9.17		− 0.799	9.87	12.13	− 1.06
Percentiles											
25	200.00	0.000	1.1000	125.0	1.70	1.48		200.0	0.00	30.00	4.05
50	400.00	0.000	1.8700	300.0	2.00	1.92		300.0	0.00	30.00	10.35
75	600.00	2.000	2.6500	475.0	5.00	2.44		500.0	0.88	30.00	20.38
Anderson–Darling normality test											
A-squared	5.14	12.76	0.439	2.83	10.55	6.65		5.62	42.86	89.51	5.91
P-value	< 0.005	< 0.005	0.286	< 0.005	< 0.005	< 0.005	< 0.005	< 0.005	< 0.005	< 0.005	< 0.005

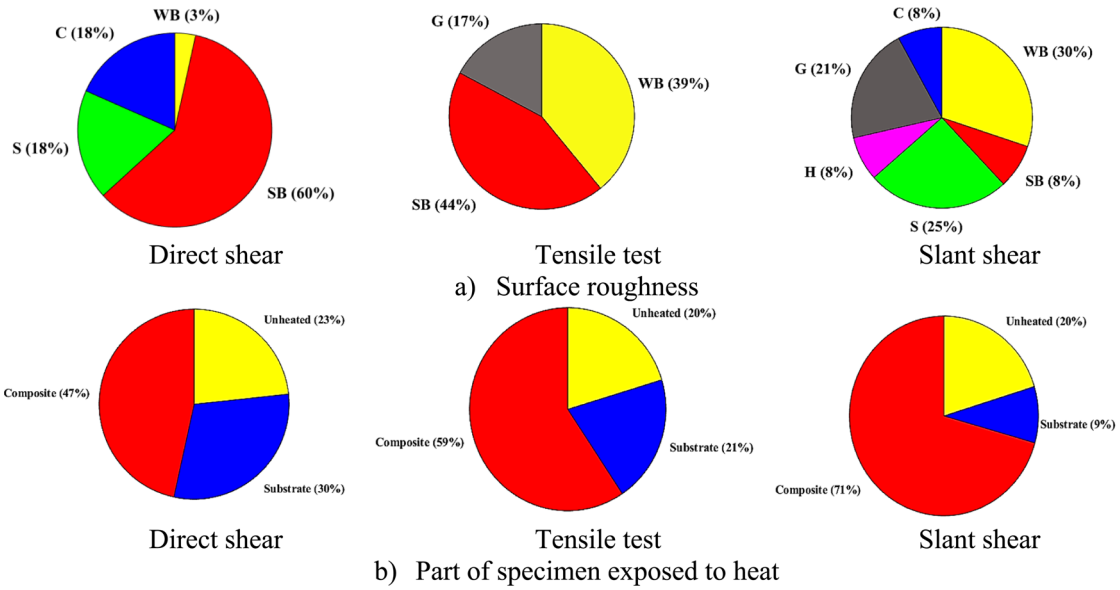

Fig. 4 Pie chart for categorical parameters

improved with surface preparation roughness, where the sandblasting (SB) displayed the highest IBS. This is attributed to raising the surface roughness, which can increase the real bonding area and greatly enhance the aggregate interlock action Chen et al. (2023). Thus, SB represents 60% and 44% of tested data in direct shear and tensile test, respectively, as shown in Fig. 4a. The results agree with the test results obtained by Haido et al. (2021) and Farouk and Jinsong (2022). On the other hand, excessive roughening resulted in a decrease in the interfacial bond strength, as shown in Fig. 5a. The same conclusion was obtained by Wang et al. (2018). Moreover, for the push-off test, there is missing data on hole and groove surface roughness as shown in Fig. 4a.

3. Although the experimental data cover a wide range of temperatures (20 up to 800 °C), there is a lack of data for temperatures higher than 600 °C, as shown in Fig. 5b, which can occur in fire tunnels (Farhangi et al., 2024). Only 23 specimens from 467 (4.9%) were tested after exposure to temperature higher than 600 °C. The low data points at temperature higher than 600 °C are due to the fact that interfacial strength is more sensitive to temperature, and higher temperatures (800 °C) cause specimen rapture, as observed by Zalhaf et al. (2024).
4. Although the fiber played an important role in improving the IBS at room temperature and after exposure to elevated temperatures as depicted in Fig. 5c, there is research gab on using fiber at temperature higher than 400 °C, as illustrated in Fig. 5d. According to the positive skewness values for fibers presented in Table 2, the normal distribution had a long tail in a positive direction, as shown in Fig. 5c. Moreover, few researches have concentrated on the IBS of concrete overlays containing fiber with a higher volume fraction (higher than 2%). The sharp beak in normal distribution for fiber in case of slant shear (Kurtosis = 9.87) demonstrated that most of data points (195 of 252) varied between 0 and 1%. This gap may be attributed to the fact that the increase in fiber content led to a decrease in concrete workability, as mentioned by (Farhangi et al., 2024; Mansour & Fayed, 2021a, b). The tensile test has approximately 48% of data points that containing fiber with volume fraction higher than 1%. Also, the percentage of specimens containing fiber with volume fracture less than 1% is about 10.5%.
5. Strengthened concrete substrate with HPC possessed a noteworthy effect on enhancing the IBS as compared to use NSC. It is seen from Fig. 5e that the most of data points presented concrete substrate strengthened with high-performance concrete (77%).
6. According to part of specimen exposed to elevated temperature, most of experimental results were obtained for composite specimen exposed to fire (269 data points) as presented in Figs. 4b and 5f, while in nature most structure members were repaired after being exposed to fire in order to meet their structural needs (Gao et al., 2018; Haddad et al., 2011). Only a few numbers of researches (Gao et al., 2018; Ouyang et al., 2023; Shang et al., 2021) have examined con-

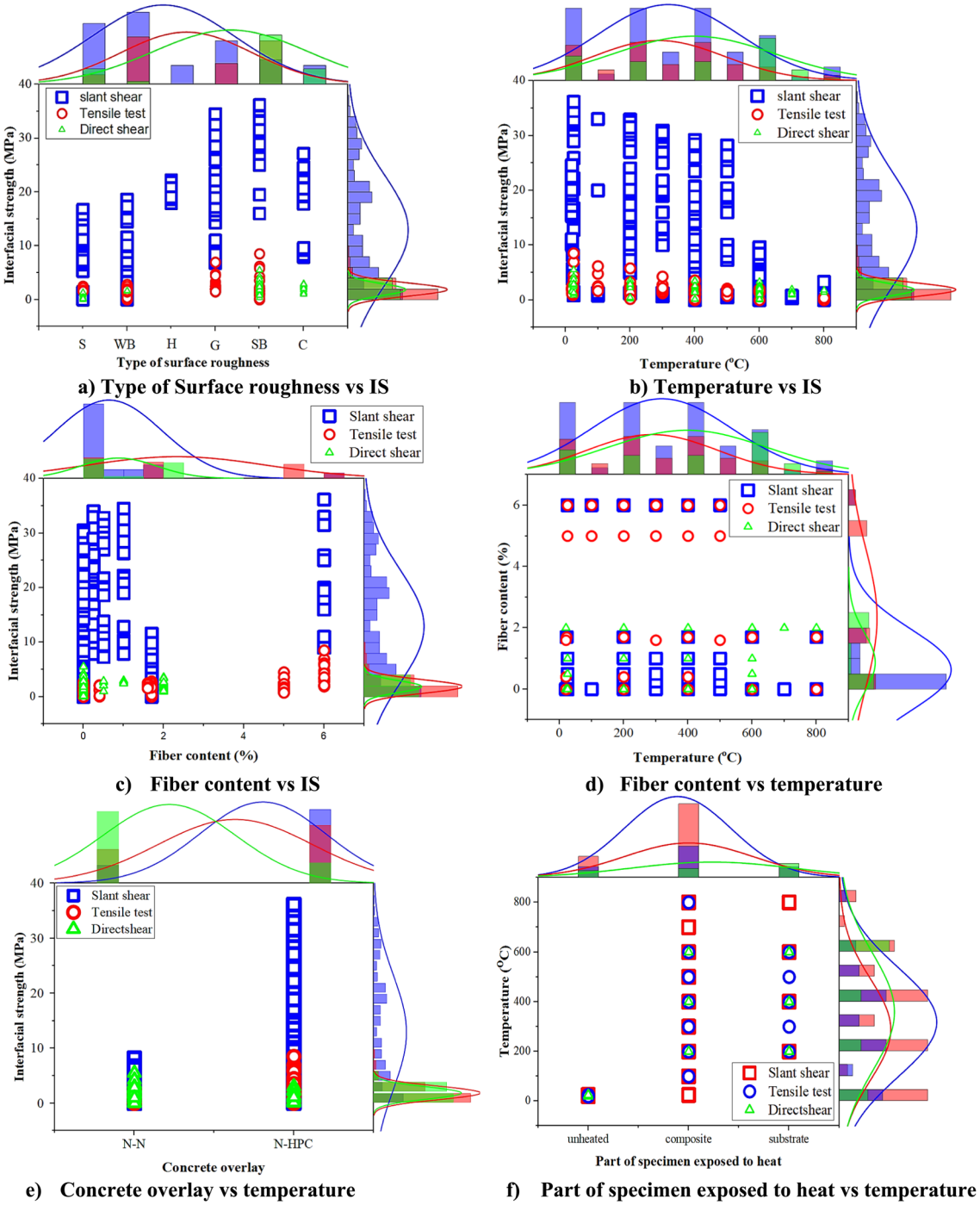

Fig. 5 Marginal plot and normal distribution for different parameters after exposure to elevated temperature

crete substrates that are heated and then reinforced with repair concrete. Thus, further experimental tests are needed for studying the effect of concrete substrate only heated on the IBS.

3 Training the ANN Model

In this research, the machine learning using feed-forward back propagation FFBP algorithm model has been constructed to study the effect of different input parameters on the interfacial bond strength (IBS) between a concrete substrate and concrete overlay after exposure to elevated

temperatures (Hagan & Menhaj, 1994). The ANN consists of three layers (an input layer, a hidden layer, and an output layer). The input layer can introduce the independent parameters as the number of neurons equals the input parameters, where each neuron has weight and bias. The summation function was used for calculating the weights (and bias) of each input parameter by using Eq. 9. Then this information is transmitted to the hidden layer, where there are three activation functions to determine the output: logsig, tansig, and purelin, as shown in Eq. 10. The accuracy of the model depends on the number of hidden layers, the number of neurons in each layer, and the activation function used (Abbas et al., 2019; Farhangi et al., 2024; Ghazy et al., 2021). Finally, the output layer presents the results:

$$z_j = \sum_i w_{ij} x_i + b_j, \tag{9}$$

$$\begin{cases} y_j = f_1(z_j) = (1 + e^{z_j})^{-1} & \text{for logsig} \\ y_j = f_2(z_j) = 2(1 + e^{-2z_j})^{-1} - 1 & \text{for tansig} \\ y_j = f_3(z_j) = z_j & \text{for pure line} \end{cases}. \tag{10}$$

The ANN model consists of three steps training, validation and test steps. The data base from literature was divided to 70% for training the ANN model, while the other 30% of data set was divided to 15% for validation step and 15% for testing the ANN. In the training step, the weights and bias values have been initiated with a random value, followed by changing the number of hidden layers and neurons to get the best performance for the ANN model. To choose the activation function, the set of input and output parameters are fixed, and the model was subjected to trials. The best performance was achieved using tansig as the activation function in both the hidden and output layers, yielding an MSE of 0.0034. It should be noted that the different scales for input features can cause some features to dominate the learning process. Thus, the input parameters are spilt to numerical and categorical features. The numerical feature includes temperature, fiber content, and shear angle, while categorical feature contains; the part of the specimen exposed to temperature (HP), type of concrete overlay (CO), concrete substrate surface preparation technique (SR). Normalization ensures all features contribute equally, leading to potentially better network performance, so min–max scaling has been used for normalizing the numerical feature and output IBS (Farhangi et al., 2024). Categorical parameters were converted into dummy variables using one-hot encoding. The second step is the validation of the ANN using the validation data set and check performance metrics. Finally, testing the ANN by comparing the predicted data with the experimental one. The performance of ANN can be defined by the mean absolute percent error (MAPE), the mean absolute error (MPE), the root mean square error (RMSE), and the coefficient of determination (R^2) between the predicted and target values (Abbas et al., 2019; Farhangi et al., 2024). The statistical measure equations and their optimal values are plotted in Table 3. The best performance was achieved when MAPE, MPE, and RMSE were equal to zero or R^2 reached 1. The ANN model is based on finding the connection between input parameters and output parameters with the minimum error. These networks' training was terminated when the number of iterations exceeded a predetermined maximum or when the smallest mean square error between the network yield and true output across all training patterns was reached (Farhangi et al., 2024). Fig. 6 presents the flowchart for ANN models.

4 Analysis

4.1 Statistical Analysis

Table 4 presents the linear correlation between the input variables and the output interfacial bond strength after

Table 3 Metrics equation and description

Metrics	Equation	Description	Critical value
MAE	$\frac{1}{n}\sum_{i=1}^{n}\lvert p_i - y_i\rvert$	Mean absolute error knows as the calculated average of errors that separates a model's forecasts from the actual values of the quantity being forecasted. The lower the MPE, the more accurate the model to estimate the experimental results	0
MAPE (%)	$\frac{1}{n}\sum_{i=1}^{n}\left\lvert\frac{p_i - y_i}{y_i}\right\rvert \times 100$	MAPE quantifies the degree to which the errors in the model's predictions are representative of the measured values by expressing their percentage. The lower the MAPE, the higher the degree of prediction	0
RMSE	$\sqrt{\frac{1}{n}\sum_{i=1}^{n}(p_i - y_i)^2}$	The root mean square error (RMSE) represents the discrepancy between the observed and anticipated data. An RMSE value near 0 results in better prediction	0
R^2	$\left[\frac{\sum_{i=1}^{n}(y_i-\overline{y})(p_i-\overline{p})}{\sqrt{\sum_{1=1}^{n}(y_i-\overline{y})^2\sum_{i=1}^{n}(p_i-\overline{p})^2}}\right]$	The coefficient of determination indicated the accuracy of the statistical model to predict the outcome. The R^2 value varies between 0 and 1. The value closer to 1 refers to superior performance	1

n is the number of experimental data, $\boldsymbol{y_i}$ and $\boldsymbol{p_i}$ are the experimental and predicted results, respectively, $\overline{\boldsymbol{y}}$ and $\overline{\boldsymbol{p}}$ are the mean of experimental and predicted data, respectively

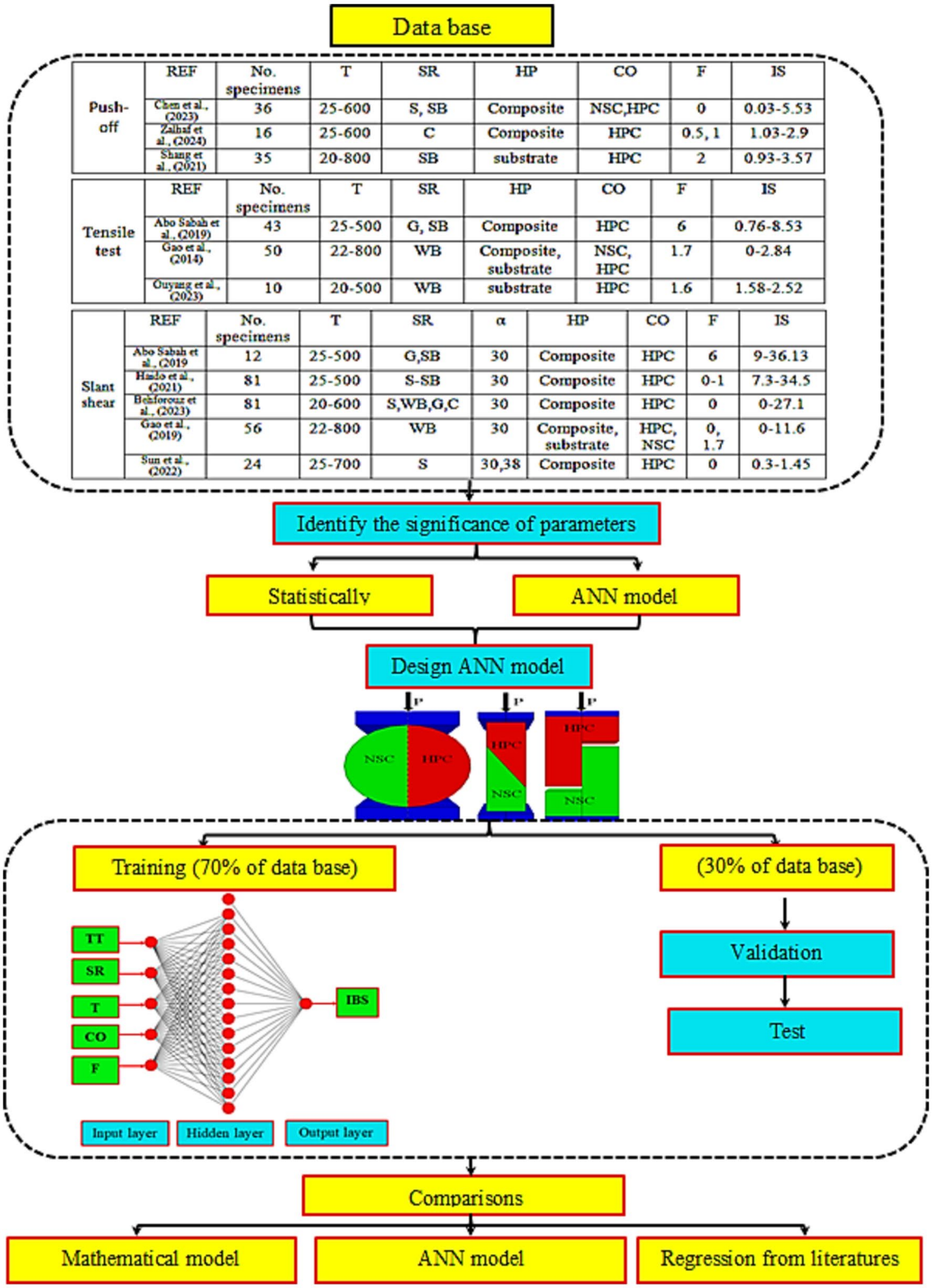

Fig. 6 Flowchart for ANN models

Table 4 Relationship between various variables and interfacial shear strength according to Pearson and Spearman rho correlations

Variables	Pearson correlation			Spearman rho		
	Pearson correlation	*P*-value	Remark	Spearman rho	*P*-value	Remark
For slant shear test						
Temperature	−0.393	< 0.001	Significant correlation and negative weak	−0.406	< 0.001	Significant correlation and negative weak
Concrete overlay	0.488	< 0.001	Significant correlation and positive strong	0.500	< 0.001	Significant correlation and positive strong
Angle	−0.291	< 0.001	Significant correlation and negative weak	−0.304	< 0.001	Significant correlation and negative weak
Heat	−0.254	< 0.001	Significant correlation and negative weak	−0.257	< 0.001	Significant correlation and negative weak
Fiber	0.16	0.011	Significant correlation and positive weak	0.247	< 0.001	Significant correlation and positive weak
Surface roughness	0.738	< 0.001	Significant correlation and positive strong	0.734	< 0.001	Significant correlation and positive strong
For tension test						
Temperature	−0.528	< 0.001	Significant correlation and negative strong	−0.549	< 0.001	Significant correlation and negative strong
Concrete overlay	0.256	0.007	Significant correlation and positive weak	0.306	0.002	Significant correlation and positive weak
Heat	−0.03	0.726	No correlation	0.181	0.132	No correlation
Fiber	0.308	0.001	Significant correlation and positive weak	0.280	0.004	Significant correlation and positive weak
Surface roughness	0.216	0.028	Significant correlation and positive weak	0.571	0.05	Significant correlation and positive weak
For direct shear test						
Temperature	−0.356	< 0.001	Significant correlation and negative weak	−0.373	< 0.001	Significant correlation and negative weak
Concrete overlay	0.184	0.044	Significant correlation and positive weak	0.157	0.146	No correlation
Heat	−0.096	0.189	No correlation	0.118	0.278	No correlation
Fiber	0.176	0.05	Less significant correlation and positive weak	0.195	0.07	No correlation
Surface roughness	0.628	< 0.001	Significant correlation and positive strong	0.527	< 0.001	Significant correlation and positive strong

exposure to elevated temperature for the three models through Pearson and Spearman rho correlations. For the two correlations, the value varied between −1 and 1. The correlation value varied between 0.5 and 1 or −0.5 and −1 refer to positive and negative strong, while 0 values indicated no correlation. Positive value means that an increase the input variable lead to improve the output-dependent variable. On the other hand, negative value indicates that an increment in the input variable had negative effect on the output variable (Kowalski, 1972). In addition, the *P*-value refers to the significant of the input variable, $P \leq 0.05$ mean a significant correlation. From the table, it can be concluded that the surface roughness is greatest significance input variable in all test technique models and has strong positive effect on the interfacial strength with Spearman rho value of 0.734, 0.571, and 0.527 for slant shear, tension and direct shear, respectively. Chen et al. (2023) concluded the same observation. Whereas an increase in temperature exposure resulted in a decrease in the interfacial bond strength, heating composite specimens showed more deterioration in the interfacial bond strength than heating concrete substrate alone. This is due to the fact that increasing temperature leads to increase the porosity at the interface between the two concrete layers, in addition to generating a variation in shrinkage at the bond contact (Gao et al., 2019), and

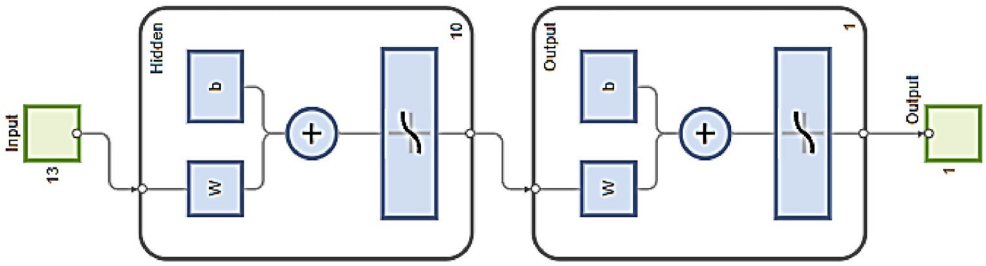

Fig. 7 The architecture of ANN model

Table 5 Sensitivity investigation of various ANNs model using feed-forward back propagation for several sets of variables

Variable	MAE	MAPE	RMSE	R^2
Direct shear test model, $n=10$, epoch = 116				
All Eq. (13)	0.365	17.24	0.08	0.916
No temperature	0.48	37.69	0.12	0.80
No heat	0.318	23.68	0.07	0.901
No fiber	0.36	27.34	0.11	0.831
No concrete type	0.30	25.96	0.113	0.87
No surface roughness	0.66	85.4	0.17	0.58
Tension test, $n=10$, epoch = 154				
All Eq. (12)	0. 23	21.4	0.03	0.973
No temperature	0.44	51.8	0.07	0.860
No heat	0.314	32.48	0.05	0.954
No fiber	0.49	31.0	0.01	0.761
No concrete type	0.168	24.4	0.04	0.950
No surface roughness	0.23	22.97	0.04	0.942
Slant shear, $n=10$, epoch = 1000				
All Eq. (11)	1.07	11.23	0.08	0.962
No temperature	2.54	29.0	0.12	0.914
No heat	1.23	16.65	0.09	0.958
No fiber	1.93	21.67	0.10	0.937
No concrete type	1.839	33.7	0.09	0.942
No surface roughness	4.39	44.29	0.17	0.792
No angle	1.17	14.62	0.07	0.972

consequently decreasing the interfacial bond strength (Ouyang et al., 2023). On the other hand, the type of concrete overlay and fiber can improve the sensitivity of the model. The Pearson correlation gives a value close to that obtained from the Spearman rho correlation, except in the case of the direct shear test, where the type of concrete overlay and fiber showed no correlation according the Spearman rho correlation.

4.2 ANN Analysis

Three ANN models are used to study the sensitivity of different parameters to the interfacial bond strength (IBS) after exposure to high temperatures. Equations (11 to 13) present the different input parameter and only output parameter in three models, which is the IBS:

$$T, \mathrm{CO}, \alpha, \mathrm{HP}, F, \mathrm{SR} \rightarrow \mathrm{IBS} \quad \text{slant shear (ANNI)}, \tag{11}$$

$$T, \mathrm{CO}, \mathrm{HP}, F, \mathrm{SR} \rightarrow \mathrm{IBS} \quad \text{tensile test(ANNII)}, \tag{12}$$

$$T, \mathrm{CO}, \mathrm{HP}, F, \mathrm{SR} \rightarrow \mathrm{IBS} \quad \text{push - off test(ANNIII)}, \tag{13}$$

where T is temperature, CO is type of concrete overlay, α is the shear angle, HP is the part of specimen exposed to temperature, F is fiber content, SR is the type of surface roughness.

In the ANN model, the sensitivity of the models were determined by calculating the effect of eliminating each input parameter in the output IBS throw MAE, MAPE, RMSE, and coefficient of determination R^2 correlations, as discussed by Abbas et al. (2019).

Fig. 7 presents the architecture of the ANN model used in the three cases, considering 10 neurons in the hidden layer by using feed-forward back propagation ANN. The results are plotted in Table 5. It can be concluded from the table that surface roughness is the most important factor in slant shear and push-off tests, while fiber content is considered the most important factor for the tension test. The elimination of these factors has an adverse effect on R^2, which was reduced from 0.966 to 0.792, 0.916 to 0.58, and 0.959 to 0.671, respectively, for slant shear, push-off, and tensile tests. The second important parameters in all tests were found to be temperature with RMSE of 0.012, 0.07, and 0.012 for direct shear tension and slant shear tests, respectively. Although the statistical model displays a significant correlation for shear angle with a P-value less than 0.05 from Pearson and Spearman rho correlations, neglecting the effect of shear angle in slant shear does not affect the IBS, where R^2 stays at 0.972. So, the shear angle can be neglected in the model. Despite the fact that the type of concrete overlay is the second sensitive variable in the push-off test according statistical analysis, it is considered the fourth significant variable in all type of tests. HP is the least important

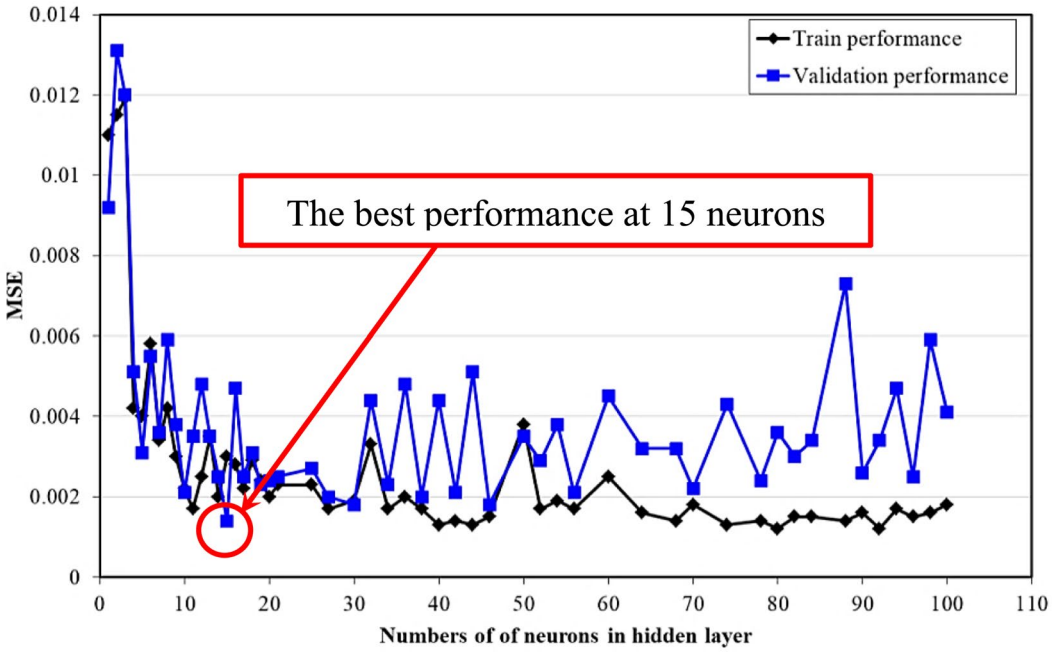

Fig. 8 MSE for train and validation performances at number of neurons varied between 1 and 100

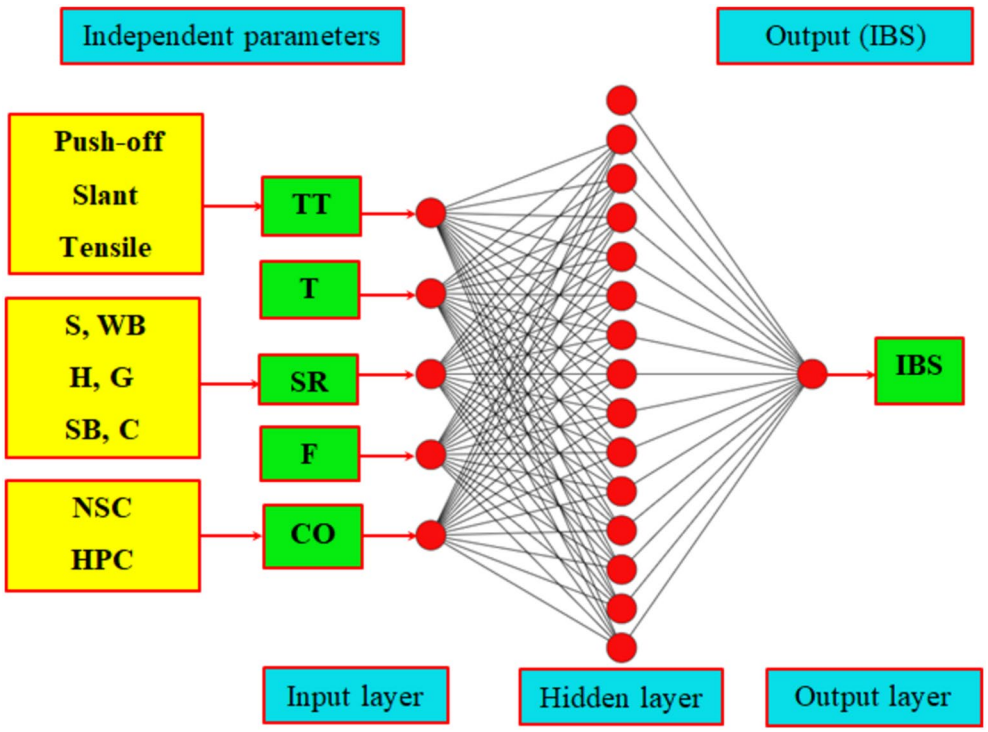

Fig. 9 Structure of the design model

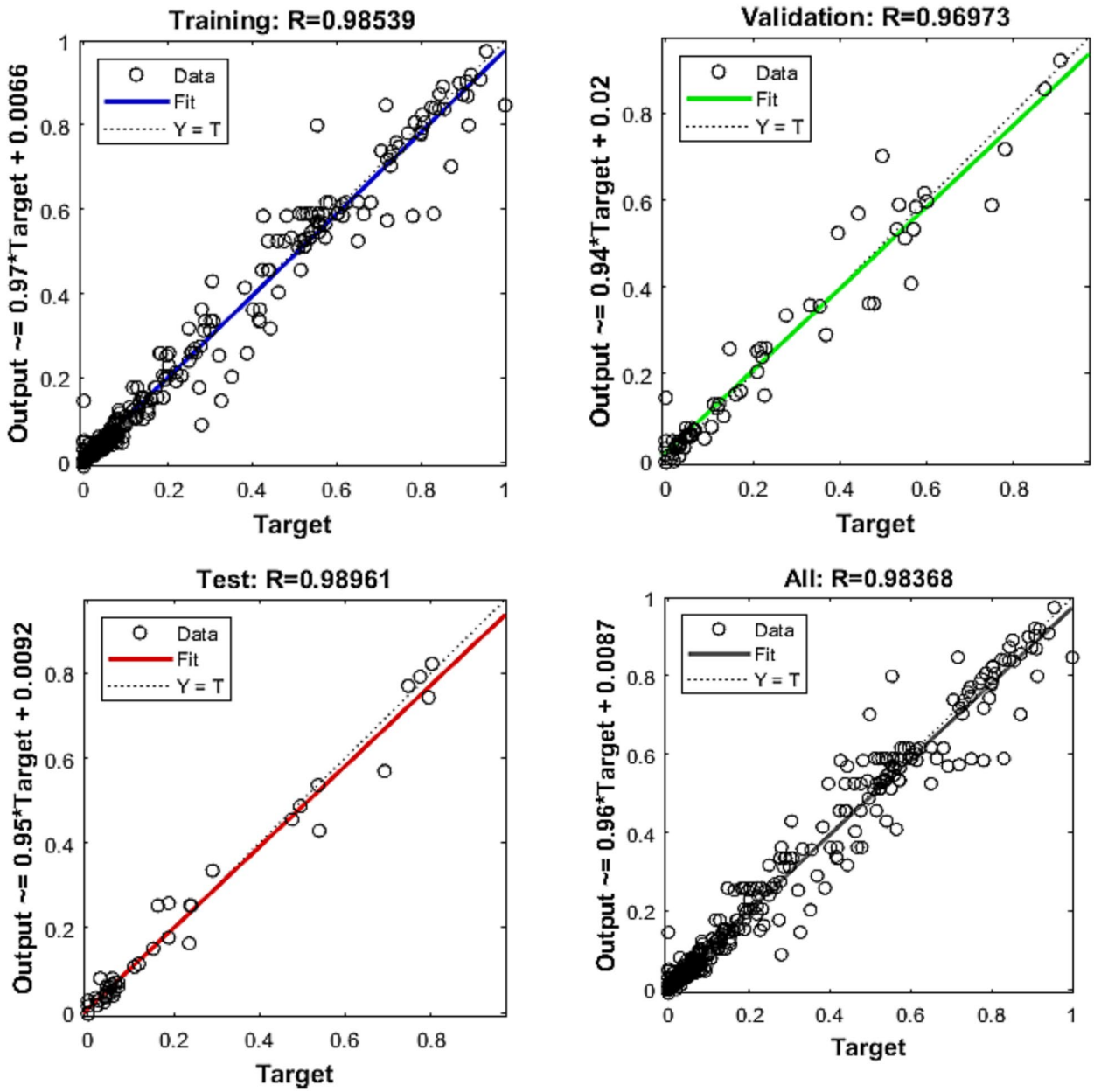

Fig. 10 Regression of the design model

factor in the ANNI and ANNII, whereas statistical analysis showed no correlation according to the *P*-value (0.189–0.726), as shown in Table 4, so it can be eliminated from the three models.

After neglecting the shear angle and HP, the arrangement of parameters according to sensitivity in order of descent in the three models is

$$\mathrm{RS}, T, F, \mathrm{CO} \rightarrow \mathrm{IBS} \qquad \text{slant shear test } \textit{ANNI}$$

$$F, T, \mathrm{RS}, \mathrm{CO} \rightarrow \mathrm{IBS} \qquad \text{tensile test ANNII}$$

$$\mathrm{RS}, T, F, \mathrm{CO} \rightarrow \mathrm{IBS} \qquad \text{Push - off test ANNIII.}$$

4.3 Designed ANN Model

As mentioned in the previous section, the interfacial bond strength significantly depends on the type of test procedure (Daneshvar et al., 2022; Momayez et al., 2005);

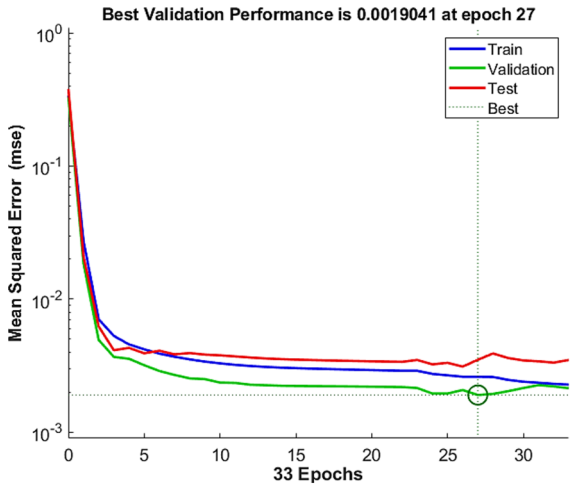

Fig. 11 Performance of the design model

a design ANN model is conducted to study the effect of including the type of test in the input parameters on the interfacial bond strength (IBS). The input parameters include the significant parameters obtained from the three ANN models, in addition to the type of test technique. The input parameters were selected based on the sensitivity analysis obtained from the three ANN models, in addition to statistical methods. These parameters are type of test (TT), type of surface roughness (RS), temperature (T), fiber content (F), and concrete overlay (CO). The output parameter is interfacial bond strength (IBS). To optimize the number of neurons in the hidden layer, the ANN model was trained with a number of neurons varied between 1 and 100. The database was split to 70% and 30% for the training and validation steps, respectively. The best behavior of ANN is that it gives the least mean square error for validation which found at a number of neurons equal to 15 as shown in Fig. 8. The structure of the ANN model is shown in Fig. 9, with one hidden layer having 15 neurons.

4.4 Performance and Validation of the Design ANN Model

The remaining data set (30% of the data) that was not introduced in training the ANN was used to validate and test the model. The accuracy of model performance during training, validation, and test results as a function of the coefficient of determination (R^2) is plotted in Fig. 10.

Table 6 Error estimation of the design model

	MAE	MAPE	RMSE	CC	R^2	Percent data for error less than 10%
Training	1.486	9.363	0.0424	0.983	0.972	95
Validation	1.147	65.273	0.0468	0.969	0.938	92.8
Test	1.001	34.06	0.0430	0.989	0.978	93.6

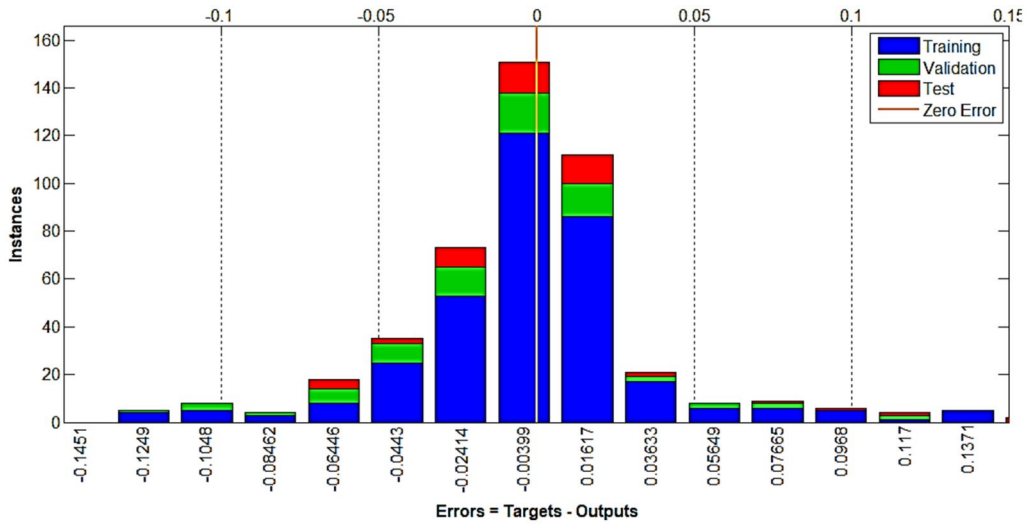

Fig. 12 The histogram of error for the design model

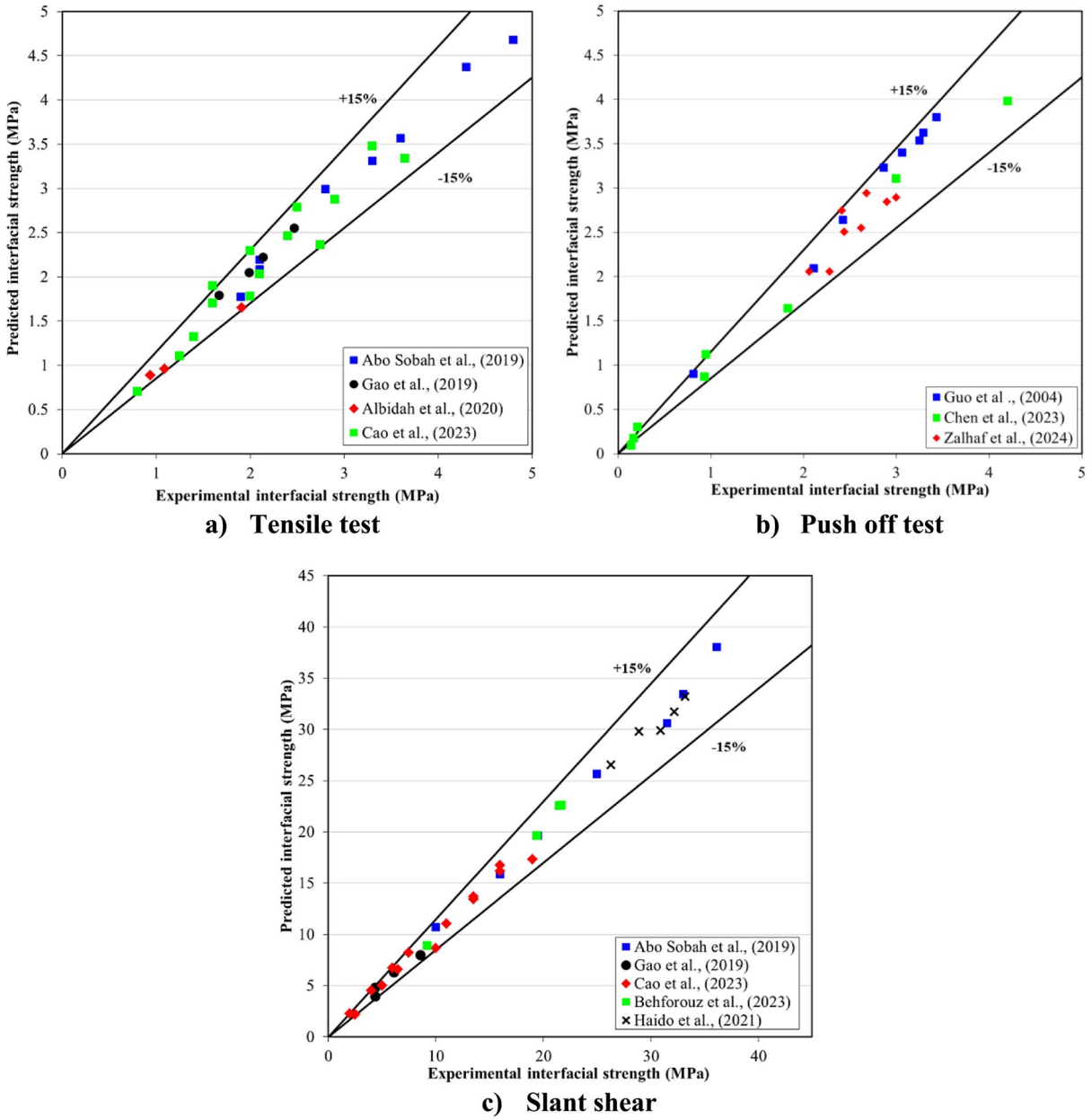

Fig. 13 Interfacial strength vs temperature for different fiber content

The performance and histogram of error are shown in Figs. 11 and 12, respectively. The output results indicated that the models work well in estimating the IBS at high temperatures, where the R^2 value is close to unity. The best performance for design ANN is plotted in Fig. 11 and Table 6. Moreover, the percentage of data with an error less than 10% equaled 95%, 92.8%, and 93.6% for training, validation, and test data, respectively (Fig. 12).

For further validation of the model in predicting the effect of input parameters on the output IBS, Fig. 13 presents a comparison between the predicted IBS and experimental results from previous studies that were not introduced in the training of the model. It can be revealed from the figures that the ANN model results agree with the experimental results, where most of the data points are limited between ±15%. The lack of data, especially in

Table 7 Connection weight and bias for design model

Weights from input layer to hidden layer (W1)														Bias (b1)
Neuron	Type of test			Surface roughness						Concrete overlay		Temperature	Fiber	
	DS	SS	T	C	G	H	S	SB	WB	HPC	NSC			
1	−0.595	0.7375	−0.589	0.4045	0.0909	−0.182	−0.184	0.0891	−0.381	0.5565	−0.793	0.2942	0.7271	1.5809
2	−0.069	−0.002	−0.525	0.337	−0.391	0.755	−0.661	0.847	1.110	0.274	0.9503	0.4804	−0.4723	1.1723
3	−0.217	−0.641	0.182	−0.257	0.3012	0.124	−0.686	−0.8117	0.911	0.627	−0.1025	−0.4894	−0.2750	1.1605
4	−0.505	0.5345	0.108	0.0607	0.606	−0.950	0.378	−0.987	−0.333	−0.056	−0.2468	−0.4662	0.31425	1.1811
5	−0.635	−0.6972	0.314	−0.359	0.388	0.650	−1.527	0.50957	0.1268	0.0065	0.9105	0.5613	−1.358	0.8319
6	−1.340	−0.437	2.567	0.2057	0.073	−0.4634	0.0415	0.0824	0.8696	−0.2360	0.7611	1.5200	−1.7303	0.4273
7	0.2107	0.7420	0.125	−0.185	−0.344	0.302	0.9393	0.06154	−0.120	−0.1175	0.8266	0.3094	0.9247	−0.159
8	0.3681	0.6233	−0.779	0.8752	−0.460	0.314	1.4407	0.0128	−0.717	−0.5271	−0.6614	−0.0440	1.9543	−0.047
9	−0.923	0.1407	0.237	0.5687	−0.633	0.354	−0.202	0.587	0.2599	0.8115	0.9283	0.16960	−0.1116	−0.374
10	0.6128	−0.663	0.647	0.4148	−1.012	−0.494	0.5824	−0.2040	−0.455	−0.3570	−0.6123	0.3214	0.3014	0.4888
11	−0.839	−0.405	0.7062	0.641	0.610	−0.874	−0.086	0.2221	−0.394	−0.1168	−0.0689	0.3559	0.1527	−0.468
12	−0.872	0.0896	0.5916	0.6788	−0.072	−0.589	0.0420	−0.652	−1.420	−0.6878	1.023	−1.3040	−0.0800	−0.664
13	−0.208	−1.7775	0.54254	0.480	−2.018	0.137	0.6481	0.4540	−0.153	−0.0046	−0.1865	−0.1457	−3.5865	1.4361
14	0.259	−0.985	1.0886	−1.120	−0.920	0.626	0.157	0.4277	0.1289	0.7340	−0.0744	1.6615	0.2678	1.5683
15	−0.352	0.4461	0.14371	0.7652	0.279	0.318	−0.109	0.27294	−0.251	0.5822	−0.5912	0.84097	0.4375	−1.710

Weights from hidden layer to output layer (W2)															Bias (b2)
1	2	3	4	5	6	7	8	9	10	11	12	13	14	15	
−1.158	−1.7187	0.6119	1.1795	0.3570	0.4183	−0.980	1.0178	−1.5334	0.6676	−2.0795	1.2404	1.1543	−0.9253	0.0774	−0.5287

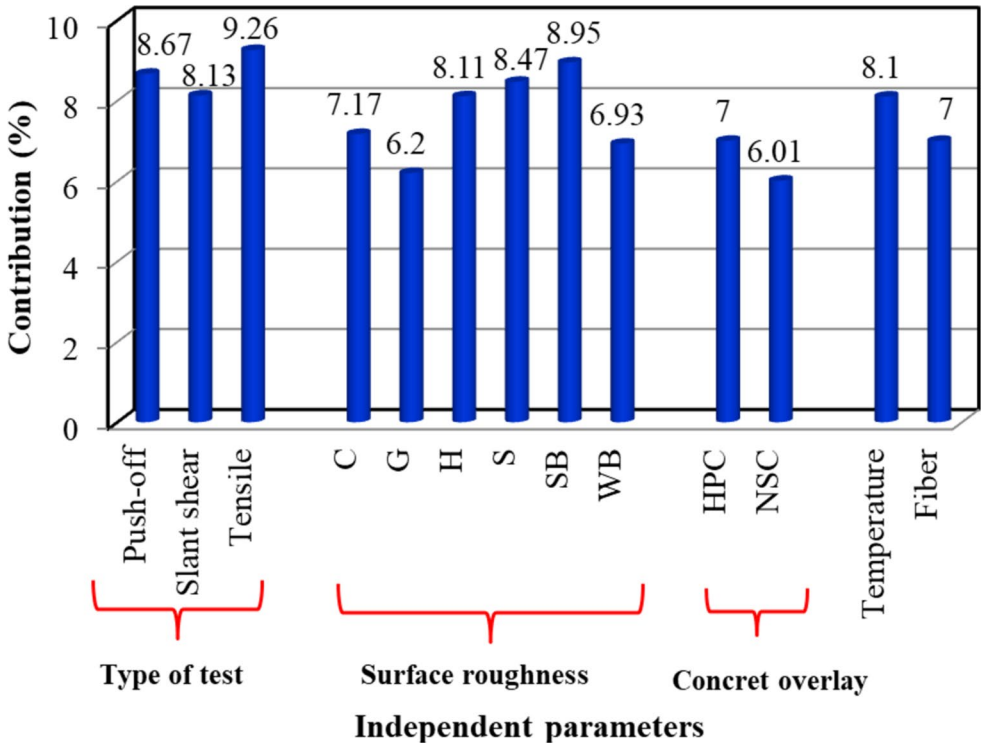

Fig. 14 The contribution of the input parameters on the output interfacial bond strength

the case of direct shear and tensile tests, resulted in some errors in predicting the IBS, as represented in Fig. 13.

4.5 Sensitivity of ANN Model

The contribution of each input parameter on output strength can be obtained by using the weight between the input and hidden layers and the weight between the hidden and output layers (Moradi et al., 2021; Nazemi et al., 2016) by using the Garson factor (Garson, 1991) Eq. 14:

$$Q_{ik} = \frac{\sum_{j=1}^{L}\left(\frac{|w_{ij}|}{\sum_{r=1}^{N}|w_{rj}|}|w_{jk}|\right)}{\sum_{i=1}^{N}\left(\sum_{j=1}^{L}\left(\frac{|w_{ij}|}{\sum_{r=1}^{N}|w_{rj}|}|w_{jk}|\right)\right)}. \quad (14)$$

Q_{ik} is the contribution of input parameters i on the output k, w_{ij} is between the input parameter i and the hidden layer neuron j,$\sum_{r=1}^{N}|w_{rj}|$ is the sum of the absolute weights between the inputs parameter and the hidden layer neuron, $|w_{jk}|$ the absolute weight between the hidden layer neuron j and the output parameter k. The connection weight and bias for the design ANN model are plotted in Table 7. The contribution of each input parameter to the output interface bond strength is plotted in Fig. 14. The results showed that the IBS is more sensitive to the type of test, surface roughness, temperature, concrete overlay and fiber.

4.6 Predicting the Unknown Data Using the Design Model

It is necessary to assess the model's accuracy in producing new findings based on novel input features, or generalizations, in line with established facts. Therefore, after training and validation of the design ANN model, the model was used for predicting the unknown data that were not in the data set. To improve the outcomes' applicability in terms of the balling impact of fiber content, the higher fiber content—more than 2%—were not included in the prediction analysis (Farhangi et al., 2024). To restrict the overall number of variables, the prediction was conducted to estimate the IS for NSC substrate strengthen with HPC overlay after exposure to different temperature exposure. Moreover, to predict the effect of fiber content on the IBS, one surface roughness was used for different test techniques. The results of the prediction data are presented in Figs. 15 and 16 for different type of test techniques. The contour lines discuss the effect of temperature exposure, surface roughness, and fiber content on the interfacial strength. The observations

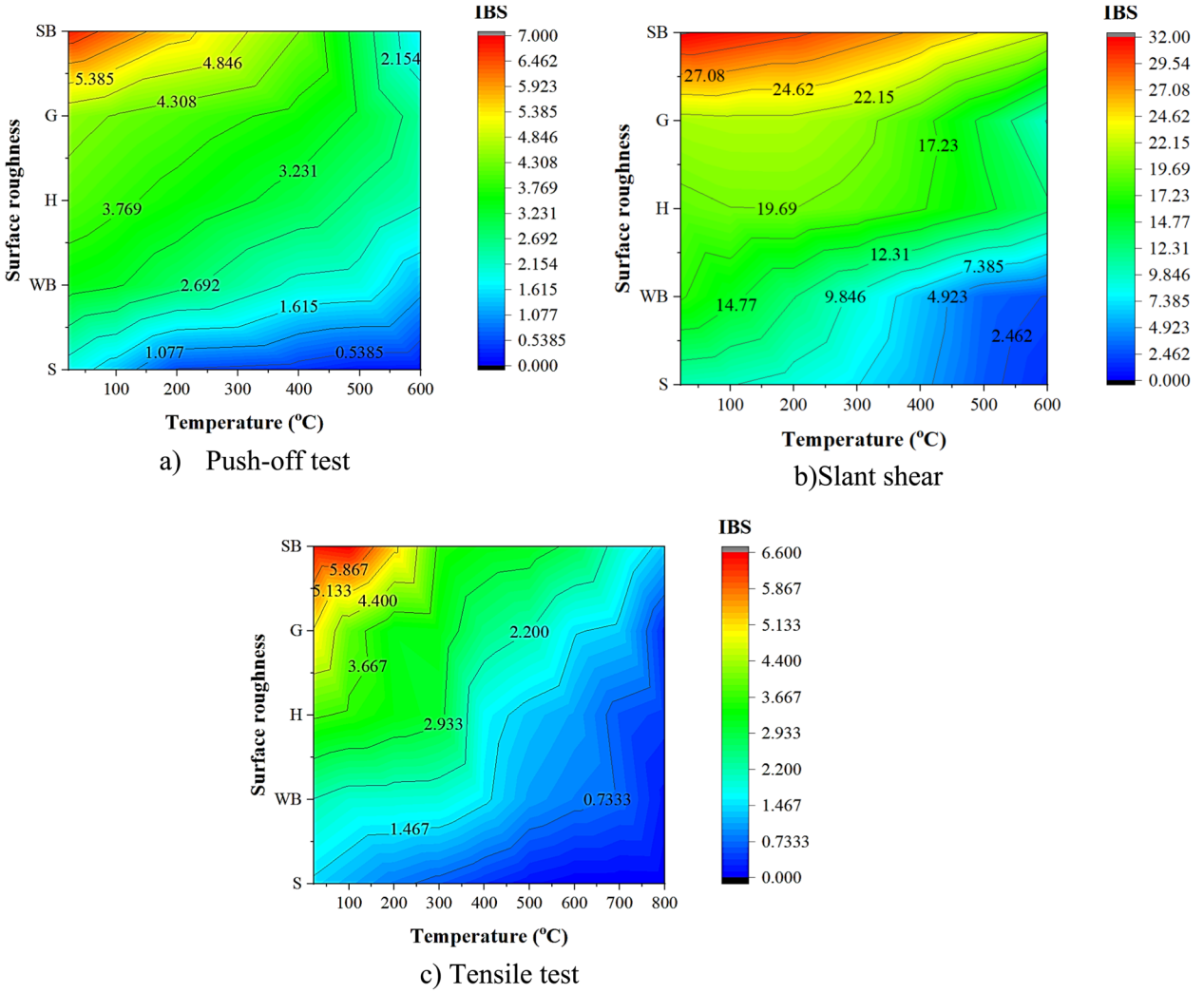

Fig. 15 Variation of interfacial strength for different surface type and temperature

show that the interfacial strength is influenced by the fiber content, interface roughness, and temperature exposure. Figs. 15 and 16 indicate that the IBS notably decrease with increasing temperature exposure for different test technique, where tensile test display more deterioration in IBS. On the other hand, slant shear recorded the least decrease in IBS, where the blue area refers to the least IBS and this region is small in slant shear. The results agree with results obtained by Chen et al. (2023). Moreover, surface roughness type significantly affected the IBS for different test techniques, where sand blasting recorded the highest IBS at different temperatures up to 800 °C. This is due to the fact that rough surface increase the mechanical interlocking and allows the concrete overlay to make shear connectors which provide significant interfacial shear strength, as discussed by Mansour and Fayd (2021a, b).

An increase in fiber content resulted in an increase the IBS at different temperatures exposure. The same trend was observed by Varona et al. (2018) who investigated that the addition of fiber can enhance the bond between reinforcement and surrounding concrete at high temperature. This is attributed to the fiber bridge the crack and delay crack propagation (Ghazy et al., 2022). Furthermore, the fibers reduced the cracks result from dry shrinkage of concrete overlay and enhance the mechanical interlock force (Jie, 2007). Additionally, the effect of fiber is more obvious in push-off test and tensile test than

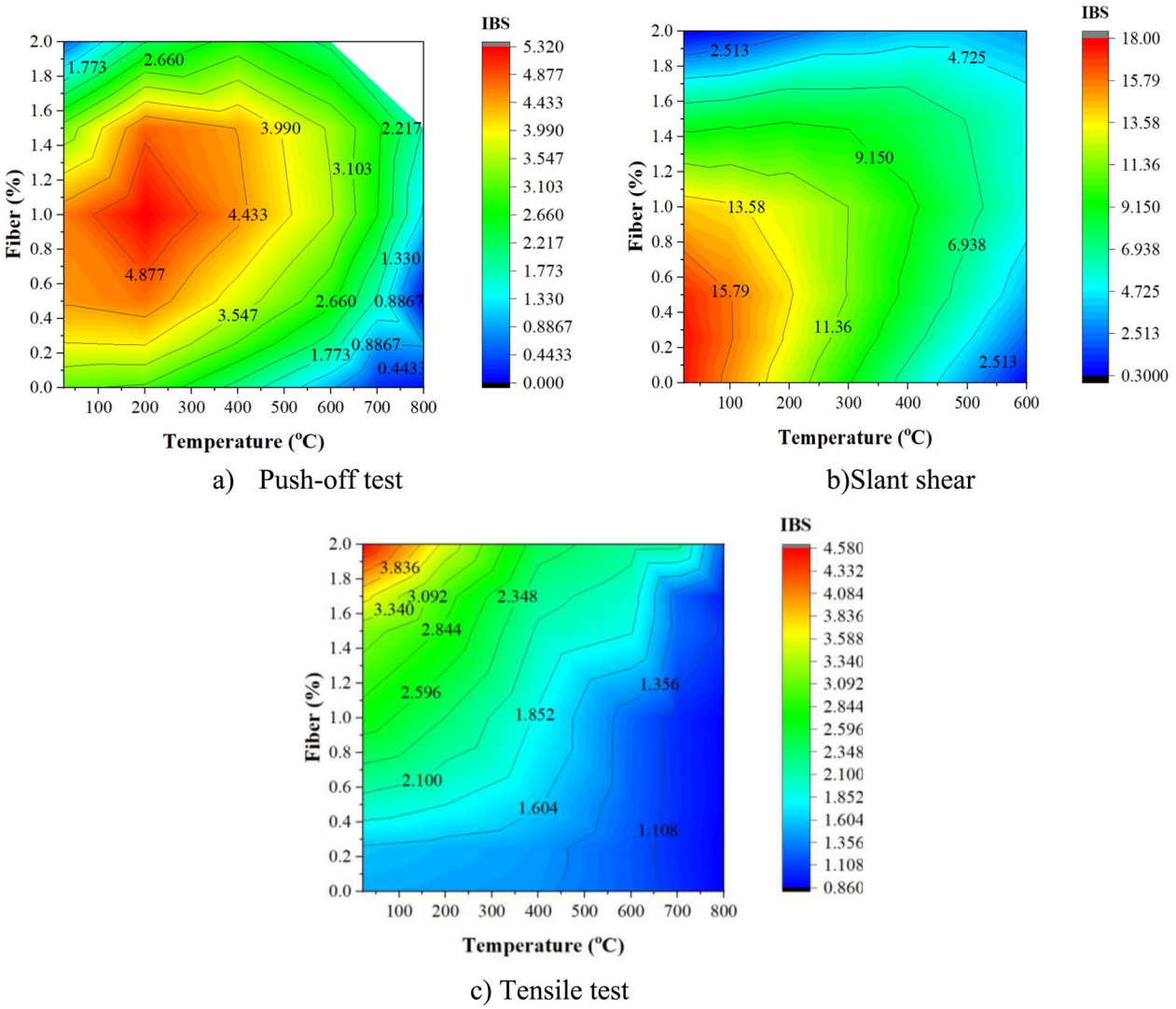

Fig. 16 Variation of interfacial strength for different fiber content and temperature

slant shear test, where increase fiber content up to 1.5% resulted in an improvement in IBS. For slant shear, the effect of fiber is noticeable at least lower fiber content. The blue area represents the least IBS, these portions are smaller in specimens with rough surface and higher fiber content.

4.7 Mathematical Model

As discussed in previous section, the IS was significantly influenced by concrete substrate surface roughness, temperature exposure, concrete overlay, and fiber content. Thus, in this investigation the coefficient of adhesion proposed by Shang et al. (2021) was modified to introduce those parameters. Data from previous studies (Chen et al., 2023; Shang et al., 2021; Zalhaf et al., 2024) were used for built the proposed IS model for direct shear test, while data obtained from (Behforouz et al., 2023; Gao et al., 2019; Haido et al., 2021) were used for built the proposed IS model for slant shear test. The IS can be anticipated by using Eqs. 15–17, considering NSC substrate strengthened with HPC overlay exposed to temperature up to 600 °C, fiber content varied from 0 to 2%, no shear connectors across the interface:

$$\mathrm{IS} = c_T c_{R,F} f_c, \tag{15}$$

Table 8 Value of constants in the design equation

Type of test	Symbol
Slant shear	$a = 3.5 \times 10^{-5}, b = 0.0391\ 0 \le T \le 200C$ $a = -7 \times 10^{-5}, b = 0.0679\ 200 \le T \le 600C$ $c = 1.795, d = 0.4, e = 2.85\ 0 \le \mathrm{SR} \le 3.5$ mm $c = -0.04, d = 0.4, e = 6.997\ 3.5 \le \mathrm{SR} \le 10$ mm
Direct shear	$a = 3 \times 10^{-5}, b = 0.061\ 0 \le T \le 200C$ $a = -6 \times 10^{-5}, b = 0.067\ 200 \le T \le 600C$ $c = 0.31, d = 0.1, e = 0.35\ 0 \le \mathrm{SR} \le 3.5$ mm $c = -0.04, d = 0.1, e = 1.257\ 3.5 \le \mathrm{SR} \le 10$ mm

$$c_T = a \times T + b_c, \tag{16}$$

$$c_{R,F} = c\mathrm{SR} + dF + e, \tag{17}$$

where c_T and $c_{R,F}$ are the coefficient of adhesion correspond to temperature, roughness, and fiber content, respectively, SR is the thick of surface roughness (mm), F is the fiber content (%), f_c is the compressive strength of concrete overlay at room temperature, a, b, c, d, e are constant depend on test type and depicted in Table 8. It can be observed from the table that, in the direct shear test, the IS was significantly influenced by surface roughness and fiber. The results agree with the results obtained from Zalhaf et al. (2024). On the other hand, temperature exposure played a significant role in the IS degradation in the case of the slant shear test.

To verify the accuracy of the proposed IS model, the proposed IS was compared with experimental data from previous studies and available empirical equations from previous studies (Chen et al., 2023; Guo et al., 2004; Santos and Júlio, 2014; Shang et al., 2021), as shown in Fig. 17. It should be noted that no empirical equation developed for IS from slant shear test in previous studies that takes into account the effect of elevated temperature and fiber content. Thus, the Santos and Júlio (2014) equation was used to predict the IS at elevated temperature by introducing the tensile strength of concrete at elevated temperature. Furthermore, the Guo et al. (2004) and Shang et al. (2021) models were applied in a range of data compatible with their authors' considerations. The ratio between the predicted and experimental IBS results has been calculated to assess the accuracy of the different regressions. For further evaluation of the accuracy of the models, the statistical parameters, including the mean, SD, and coefficient of variation (CV), coefficient of correlation (CC), and coefficient of determination (R^2) were calculated and depicted in Table 9. The results revealed that the proposed IS was able to predict the IS with coefficient of correlation (CC) values of 0.95 and 0.82 for slant shear and direct shear tests, respectively. Moreover, it can be observed from the figure that the majority of the data are within ± 20% ranges. The Santos and Júlio (2014) and Chen et al. (2023) equation values were found to be lower than experimental results in the case of slant shear. On the other hand, the Gou et al. (2004) model gave the

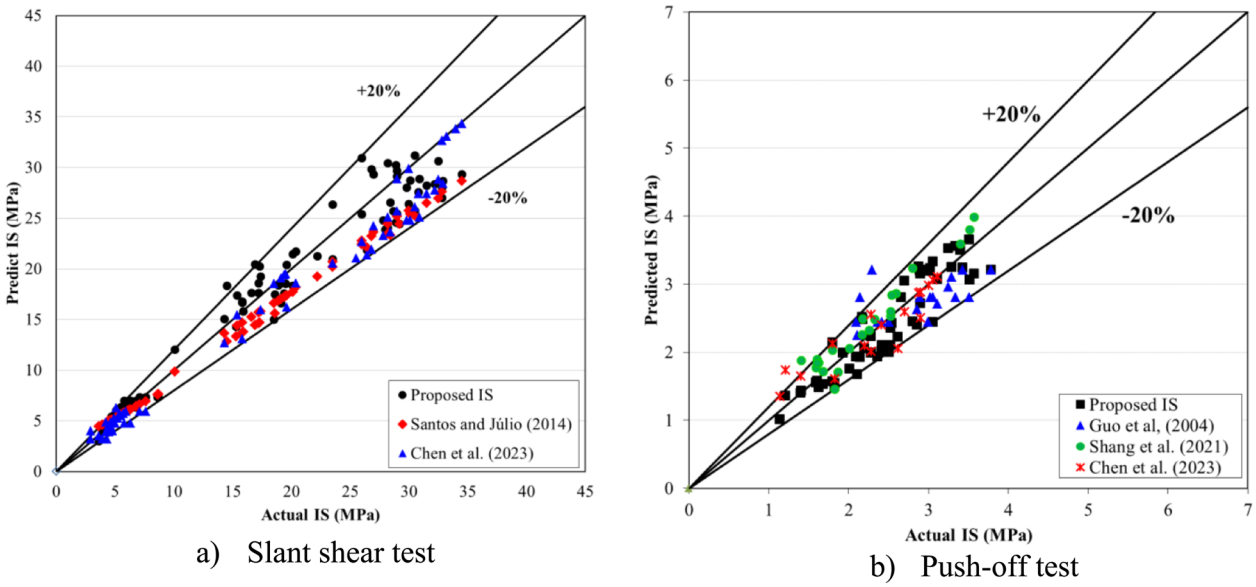

Fig. 17 Comparison between different models and design IS

Table 9 Statistical parameters for the assessment of models

Statistical parameters for $\frac{IS_{pred}}{IS_{Exp}}$								
	Mean	**SD**	**Variance**	**CV**	**Min. value**	**Max. value**	**CC**	R^2
Proposed IBS for slant shear	0.995	0.114	0.013	0.116	0.81	1.261	0.95	0.90
Proposed IBS for direct shear test	0.954	0.115	0.013	0.120	0.756	1.19	0.82	0.66
Santos and Júlio (2014)	0.85	0.052	0.002	0.61	0.76	0.97	0.84	0.72
Chen et al. (2023) for direct shear	0.97	0. 13	0.018	0.13	0.78	1.18	0.92	0.84
Chen et al. (2023) for slant shear	0.99	0.074	0.02	0.127	0.87	1.27	0.957	0.91
Shang et al. (2021)	1.07	0.103	0.010	0.096	0.905	1.17	0.96	0.92
Guo et al. (2004)	0.98	0.159	0.025	0.162	0.953	1.39	0.76	0.577

SD is the standard deviation, CV is the coefficient of variance, CC coefficient of correlation, R^2 is the coefficient of determination

Table 10 Experimental to predicted IS for different models after exposure to elevated temperature

	Experimental Cao et al. (2023)	**ANN model**	**Proposed IS model**	$\frac{IBS_{ANN}}{IBS_{Exp}}$	$\frac{IBS_{proposedISmodel}}{IBS_{Exp}}$
20	17.5	18.33	15.2	1.05	0.87
200	15	16.21	15.5	1.08	1.01
400	12.5	12.78	13.24	1.02	1.06
600	6.5	7.80	7.34	1.2	1.12
800	2.5	2.68	1.43	1.07	0.57
Mean				1.08	0.926
Standard deviation				0.071	0.219
Co-efficient of variation				0.065	0.236

lowest accuracy, with a CC equal to 0.76 in the direct shear test.

For validating the ANN model and design IBS models, the experimental IBS obtained from Cao et al., (2023) for slant shear test has been used for assessing the predicted IBS from the ANN model and the proposed IS model for slant shear. The ratio of predicted IBS to experimental IBS for different models is plotted in Table 10. From the result it is clear that the ANN model gave a good accuracy at different temperature exposures with the least coefficient of variance of 0.057. The prediction based on the proposed IS model gave suitable results up to 600 °C, where the equation was designed to predict IBS up to temperature of 600 °C, after that the predicted IS is lower than that of experimental results.

5 Conclusions

The interfacial bond strength (IBS) after exposure to elevated temperature can be obtained using different test bond techniques including tensile test, direct shear test, and slant shear test. Thus, the data obtained from previous studies are divided into three groups according to test technique. Firstly, the data obtained from previous studies have been analyzed using statistical analysis to assess the effect of various independent parameters on the IBS for different tests. Also, three artificial neural network (ANN) models have been conducted to study the effect of different independent parameters on the IBS after exposure to elevated temperature. After that, a design ANN model has been proposed to predict the interfacial bond strength with input parameters including type of test, surface roughness, temperature, type of concrete overlay, and fiber content. The input parameters were selected based on the sensitivity analysis obtained from the three ANN models, in addition to statistical methods. Finally, a mathematical IBS equation has been developed to predict the IBS between NSC substrate and HPC overlay after exposure to high temperature. The design ANN model and mathematical IBS equation were compared with available regressions obtained from the literature. The summary of conclusions is depicted as follows:

1. The ANN model was able to assess the effect of each independent input parameter on the IBS after exposure to a temperature.
2. The feed-forward backpropagation ANN with one hidden layer containing 15 neurons produced the best results, achieving RMSE and R^2 values of (0.0424, 0.972), (0.0468, 0.938), and (0.0430, 0.978) for training, validation, and testing, respectively.
3. Based on the ANN design analysis, the test technique was identified as the most influential parameter affecting the IBS after exposure to elevated temperatures, followed by surface roughness. In contrast, fiber content was found to have the least impact.

4. The ANN model demonstrated high accuracy in predicting the interfacial bond strength between normal-strength concrete and high-performance concrete overlays after exposure to elevated temperatures, achieving an R^2 value of 0.979. This level of accuracy is particularly noteworthy, as the data were collected from multiple research studies using various testing techniques, underscoring the ANN model's capability to effectively predict interfacial bond strength under diverse conditions.
5. Generalization analysis indicated that the interface surface roughness significantly enhances the IBS. Besides, inclusion of fiber can improve the IBS after exposure to high temperature.
6. Temperature exposure had an adverse effect on the IBS, where the tensile test results were the most sensitive to elevated temperature based on the Person correlation value of −0.528.
7. The proposed IBS model demonstrated a high accuracy in predicting the IBS between NSC and HPC overlay after exposure to elevated temperature in case of under combined stress with coefficient of determination R^2 of 0.90.
8. The regression obtained by Chen et al. (2023) can be used for predicting the IBS between NSC and HPC after exposure to temperature up to 400 °C with an R^2 equal to 0.84.
9. The designed ANN and proposed IBS models demonstrated a solid understanding of how elevated temperatures affect interfacial bond strength, as well as how surface roughness types and fiber content can enhance this bond. This information is valuable for designers modeling the shear behavior of reinforced concrete members strengthened with concrete overlays.
10. This research effectively bridges the gaps in both theoretical and experimental findings by integrating ANN models with advanced computational techniques and robust statistical analyses. This multifaceted approach not only enriches our understanding of the topic, but also provides more precise insights and predictive capabilities.
11. Assessing the interfacial bond strength between the two concrete layers after fire exposure is crucial for evaluating the overall fire performance, which is essential for the structural fire design of composite concrete layers.
12. Based on the data collected from previous studies, further experimental investigations are necessary to understand the impact of different test techniques on interfacial bond strength after exposure to high temperatures, particularly in direct shear and tensile tests.
13. There is a noticeable lack of data regarding the use of fibers with varying content, especially at temperatures exceeding 400 °C. To enhance the accuracy of the proposed IBS models, more experimental data are required.
14. Additional studies are needed to fully comprehend the behavior of concrete substrates subjected to high temperatures and subsequently repaired with high-performance concrete.

Appendix: Data base from previous studies

Refs.	Type of test	*T*	SR	*α*	HP	CO	*F*	IBS
Abo Sabah et al. (2019)	Slant shear	25	Groove	30	Non	N-HPC	6	25.9
		100	Groove	30	Composite	N-HPC	6	20
		200	Groove	30	Composite	N-HPC	6	18
		300	Groove	30	Composite	N-HPC	6	16
		400	Groove	30	Composite	N-HPC	6	11
		500	Groove	30	Composite	N-HPC	6	9
		25	SB	30	Non	N-HPC	6	36.13
		100	SB	30	Composite	N-HPC	6	33
		200	SB	30	Composite	N-HPC	6	31.5
		300	SB	30	Composite	N-HPC	6	25
		400	SB	30	Composite	N-HPC	6	19.5
		500	SB	30	Composite	N-HPC	6	16
Haido et al. (2021)	Slant shear	25	S	30	Unheated	N-HPC	0	15.1
		200	S	30	Composite	N-HPC	0	14
		300	S	30	Composite	N-HPC	0	12.7
		400	S	30	Composite	N-HPC	0	11.8
		500	S	30	Composite	N-HPC	0	10.1
		25	S	30	Composite	N-HPC	0.25	16.7
		200	S	30	Composite	N-HPC	0.25	15
		300	S	30	Composite	N-HPC	0.25	13.3
		400	S	30	Composite	N-HPC	0.25	9
		500	S	30	Composite	N-HPC	0.25	7.9
		25	S	30	Unheated	N-HPC	0.5	13.8
		200	S	30	Composite	N-HPC	0.5	12
		300	S	30	Composite	N-HPC	0.5	10.8
		400	S	30	Composite	N-HPC	0.5	9.5
		500	S	30	Composite	N-HPC	0.5	7.3
		25	S	30	Unheated	N-HPC	1	12.8
		200	S	30	Composite	N-HPC	1	10.3
		300	S	30	Composite	N-HPC	1	10
		400	S	30	Composite	N-HPC	1	8
		500	S	30	Composite	N-HPC	1	7.9
		25	SB	30	Unheated	N-HPC	0	30.5
		200	SB	30	Composite	N-HPC	0	29
		300	SB	30	Composite	N-HPC	0	28.9
		400	SB	30	Composite	N-HPC	0	28.7
		500	SB	30	Composite	N-HPC	0	26.3
		25	SB	30	Unheated	N-HPC	0.25	34
		200	SB	30	Composite	N-HPC	0.25	32.9
		300	SB	30	Composite	N-HPC	0.25	29
		400	SB	30	Composite	N-HPC	0.25	27.8
		500	SB	30	Composite	N-HPC	0.25	25.5
		25	SB	30	Unheated	N-HPC	0.5	32.8
		200	SB	30	Composite	N-HPC	0.5	30.8
		300	SB	30	Composite	N-HPC	0.5	29.8

Refs.	Type of test	*T*	SR	*α*	HP	CO	*F*	IBS
		400	SB	30	Composite	N-HPC	0.5	28
		500	SB	30	Composite	N-HPC	0.5	27
		25	SB	30	Unheated	N-HPC	1	33.2
		200	SB	30	Composite	N-HPC	1	32.2
		300	SB	30	Composite	N-HPC	1	30.9
		400	SB	30	Composite	N-HPC	1	30.5
		500	SB	30	Composite	N-HPC	1	29
		25	G	30	Unheated	N-HPC	0	30
		200	G	30	Composite	N-HPC	0	28.2
		300	G	30	Composite	N-HPC	0	26
		400	G	30	Composite	N-HPC	0	23.5
		500	G	30	Composite	N-HPC	0	20.4
		25	G	30	Unheated	N-HPC	0.25	29
		200	G	30	Composite	N-HPC	0.25	27
		300	G	30	Composite	N-HPC	0.25	26.8
		400	G	30	Composite	N-HPC	0.25	26
		500	G	30	Composite	N-HPC	0.25	23.5
		25	G	30	Unheated	N-HPC	0.5	32.8
		200	G	30	Composite	N-HPC	0.5	31.5
		300	G	30	Composite	N-HPC	0.5	30.1
		400	G	30	Composite	N-HPC	0.5	29.2
		500	G	30	Composite	N-HPC	0.5	28.2
		25	G	30	Unheated	N-HPC	1	34.5
		200	G	30	Composite	N-HPC	1	32.5
		300	G	30	Composite	N-HPC	1	30.5
		400	G	30	Composite	N-HPC	1	28.4
		500	G	30	Composite	N-HPC	1	26.4
		25	H	30	Unheated	N-HPC	0	20.3
		200	H	30	Composite	N-HPC	0	19.9
		300	H	30	Composite	N-HPC	0	19
		400	H	30	Composite	N-HPC	0	18.4
		500	H	30	Composite	N-HPC	0	17.9
		25	H	30	Unheated	N-HPC	0.25	20.8
		200	H	30	Composite	N-HPC	0.25	20.2
		300	H	30	Composite	N-HPC	0.25	19.5
		400	H	30	Composite	N-HPC	0.25	19.4
		500	H	30	Composite	N-HPC	0.25	18.9
		25	H	30	Unheated	N-HPC	0.5	21.7
		200	H	30	Composite	N-HPC	0.5	20.1
		300	H	30	Composite	N-HPC	0.5	20
		400	H	30	Composite	N-HPC	0.5	19.8
		500	H	30	Composite	N-HPC	0.5	18.6
		25	H	30	Unheated	N-HPC	1	22.2
		200	H	30	Composite	N-HPC	1	22
		300	H	30	Composite	N-HPC	1	21.8
		400	H	30	Composite	N-HPC	1	20.7
		500	H	30	Composite	N-HPC	1	19
Behforouz et al. (2023)	Slant shear	20	S	30	Unheated	N-HPC	0	10
		200	S	30	Composite	N-HPC	0	5.3
		400	S	30	Composite	N-HPC	0	0
		600	S	30	Composite	N-HPC	0	0

Refs.	Type of test	*T*	SR	*α*	HP	CO	*F*	IBS
		20	S	30	Unheated	N-HPC	0	10.5
		200	S	30	Composite	N-HPC	0	6.6
		400	S	30	Composite	N-HPC	0	0
		600	S	30	Composite	N-HPC	0	0
		20	S	30	Unheated	N-HPC	0	10.4
		200	S	30	Composite	N-HPC	0	6.5
		400	S	30	Composite	N-HPC	0	0
		600	S	30	Composite	N-HPC	0	0
		20	S	30	Unheated	N-HPC	0	10.9
		200	S	30	Composite	N-HPC	0	6.8
		400	S	30	Composite	N-HPC	0	0
		600	S	30	Composite	N-HPC	0	0
		20	S	30	Unheated	N-HPC	0	11.1
		200	S	30	Composite	N-HPC	0	7.3
		400	S	30	Composite	N-HPC	0	0
		600	S	30	Composite	N-HPC	0	0
		20	WB	30	Unheated	N-HPC	0	15.3
		200	WB	30	Composite	N-HPC	0	10.1
		400	WB	30	Composite	N-HPC	0	0
		600	WB	30	Composite	N-HPC	0	0
		20	WB	30	Unheated	N-HPC	0	15.9
		200	WB	30	Composite	N-HPC	0	14.5
		400	WB	30	Composite	N-HPC	0	2.2
		600	WB	30	Composite	N-HPC	0	0
		20	WB	30	Unheated	N-HPC	0	15.8
		200	WB	30	Composite	N-HPC	0	15.1
		400	WB	30	Composite	N-HPC	0	2.8
		600	WB	30	Composite	N-HPC	0	0
		20	WB	30	Unheated	N-HPC	0	17.2
		200	WB	30	Composite	N-HPC	0	16.9
		400	WB	30	Composite	N-HPC	0	2.4
		600	WB	30	Composite	N-HPC	0	0
		20	WB	30	Unheated	N-HPC	0	18.6
		200	WB	30	Composite	N-HPC	0	17.3
		400	WB	30	Composite	N-HPC	0	3.2
		600	WB	30	Composite	N-HPC	0	0
		20	C	30	Unheated	N-HPC	0	20.8
		200	C	30	Composite	N-HPC	0	18.8
		400	C	30	Composite	N-HPC	0	17.8
		600	C	30	Composite	N-HPC	0	7.9
		20	C	30	Unheated	N-HPC	0	21.1
		200	C	30	Composite	N-HPC	0	20.5
		400	C	30	Composite	N-HPC	0	19.2
		600	C	30	Composite	N-HPC	0	8.3
		20	C	30	Unheated	N-HPC	0	21.5
		200	C	30	Composite	N-HPC	0	21.7
		400	C	30	Composite	N-HPC	0	19.4
		600	C	30	Composite	N-HPC	0	9.2
		20	C	30	Unheated	N-HPC	0	22.5
		200	C	30	Composite	N-HPC	0	24
		400	C	30	Composite	N-HPC	0	20.7

Refs.	Type of test	*T*	SR	*α*	HP	CO	*F*	IBS
		600	C	30	Composite	N-HPC	0	9.3
		20	C	30	Unheated	N-HPC	0	24.6
		200	C	30	Composite	N-HPC	0	27.1
		400	C	30	Composite	N-HPC	0	20.6
		600	C	30	Composite	N-HPC	0	9.6
		20	G	30	Unheated	N-HPC	0	18.5
		200	G	30	Composite	N-HPC	0	15.4
		400	G	30	Composite	N-HPC	0	14.3
		600	G	30	Composite	N-HPC	0	6.8
		20	G	30	Unheated	N-HPC	0	19.1
		200	G	30	Composite	N-HPC	0	17.4
		400	G	30	Composite	N-HPC	0	15.8
		600	G	30	Composite	N-HPC	0	7.1
		20	G	30	Unheated	N-HPC	0	19.4
		200	G	30	Composite	N-HPC	0	19.6
		400	G	30	Composite	N-HPC	0	16.6
		600	G	30	Composite	N-HPC	0	7.3
		20	G	30	Unheated	N-HPC	0	19.5
		200	G	30	Composite	N-HPC	0	20.1
		400	G	30	Composite	N-HPC	0	17.2
		600	G	30	Composite	N-HPC	0	7.6
		20	G	30	Unheated	N-HPC	0	20.1
		200	G	30	Composite	N-HPC	0	22.2
		400	G	30	Composite	N-HPC	0	18.9
		600	G	30	Composite	N-HPC	0	8.4
Gao et al. (2019)	Slant shear	22	WB	30	Unheated	N–N	0	5.5
		22	WB	30	Unheated	N–N	0	8.2
		22	WB	30	Unheated	N–N	0	5.1
		200	WB	30	Composite	N–N	0	5.2
		200	WB	30	Composite	N–N	0	4.9
		200	WB	30	Composite	N–N	0	6.8
		400	WB	30	Composite	N–N	0	5.5
		400	WB	30	Composite	N–N	0	4.7
		400	WB	30	Composite	N–N	0	4.7
		600	WB	30	Composite	N–N	0	3.6
		800	WB	30	Composite	N–N	0	0
		22	WB	30	Unheated	N-HPC	1.7	5.5
		22	WB	30	Unheated	N-HPC	1.7	5.5
		22	WB	30	Unheated	N-HPC	1.7	4
		200	WB	30	Composite	N-HPC	1.7	7.6
		200	WB	30	Composite	N-HPC	1.7	5.9
		200	WB	30	Composite	N-HPC	1.7	7.1
		400	WB	30	Composite	N-HPC	1.7	4.2
		400	WB	30	Composite	N-HPC	1.7	4.6
		400	WB	30	Composite	N-HPC	1.7	6.2
		600	WB	30	Composite	N-HPC	1.7	2.9
		600	WB	30	Composite	N-HPC	1.7	4.8
		600	WB	30	Composite	N-HPC	1.7	2.9
		800	WB	30	Composite	N-HPC	1.7	2.9
		800	WB	30	Composite	N-HPC	1.7	0.6
		800	WB	30	Composite	N-HPC	1.7	0.6

Refs.	Type of test	*T*	SR	*α*	HP	CO	*F*	IBS
		800	WB	30	Composite	N-HPC	1.7	1
		22	WB	30	Unheated	N–N	0	5.4
		22	WB	30	Unheated	N–N	0	5.7
		22	WB	30	Unheated	N–N	0	5.4
		200	WB	30	Substrate	N–N	0	5
		200	WB	30	Substrate	N–N	0	5.8
		200	WB	30	Substrate	N–N	0	6.3
		400	WB	30	Substrate	N–N	0	4.3
		400	WB	30	Substrate	N–N	0	3
		400	WB	30	Substrate	N–N	0	4.2
		600	WB	30	Substrate	N–N	0	4.3
		600	WB	30	Substrate	N–N	0	3.9
		600	WB	30	Substrate	N–N	0	3.9
		800	WB	30	Substrate	N–N	0	0.7
		800	WB	30	Substrate	N–N	0	0
		22	WB	30	Unheated	N-HPC	1.7	4.4
		22	WB	30	Unheated	N-HPC	1.7	3.9
		22	WB	30	Unheated	N-HPC	1.7	3.9
		200	WB	30	Substrate	N-HPC	1.7	8.7
		200	WB	30	Substrate	N-HPC	1.7	8.6
		200	WB	30	Substrate	N-HPC	1.7	11.6
		400	WB	30	Substrate	N-HPC	1.7	9.9
		400	WB	30	Substrate	N-HPC	1.7	6.1
		400	WB	30	Substrate	N-HPC	1.7	6.8
		600	WB	30	Substrate	N-HPC	1.7	4.4
		600	WB	30	Substrate	N-HPC	1.7	5.1
		600	WB	30	Substrate	N-HPC	1.7	4.5
		800	WB	30	Substrate	N-HPC	1.7	0
		800	WB	30	Substrate	N-HPC	1.7	3.3
		800	WB	30	Substrate	N-HPC	1.7	0
Sun et al. (2022)	Slant shear	25	S	30	Unheated	N–N	0	0.9
		100	S	30	Composite	N–N	0	0.8
		200	S	30	Composite	N–N	0	1.17
		300	S	30	Composite	N–N	0	0.67
		400	S	30	Composite	N–N	0	0.55
		500	S	30	Composite	N–N	0	0.48
		600	S	30	Composite	N–N	0	0.37
		700	S	30	Composite	N–N	0	0.3
		25	S	38	Unheated	N–N	0	1.133333
		100	S	38	Composite	N–N	0	1.02
		200	S	38	Composite	N–N	0	1.4
		300	S	38	Composite	N–N	0	0.96
		400	S	38	Composite	N–N	0	0.89
		500	S	38	Composite	N–N	0	0.9
		600	S	38	Composite	N–N	0	0.58
		700	S	38	Composite	N–N	0	0.51
		25	S	38	Unheated	N–N	0	1.455556
		100	S	38	Composite	N–N	0	1.31
		200	S	38	Composite	N–N	0	1.44
		300	S	38	Composite	N–N	0	1.27
		400	S	38	Composite	N–N	0	1.02

Refs.	Type of test	*T*	SR	*α*	HP	CO	*F*	IBS
		500	S	38	Composite	N–N	0	0.96
		600	S	38	Composite	N–N	0	0.81
		700	S	30	Composite	N–N	0	0.78
Chen et al. (2023)	Push-off test	20	SB	–	Unheated	N–N	0	3.06
		200	SB	–	Composite	N–N	0	2.28
		400	SB	–	Composite	N–N	0	2.2
		600	SB	–	Composite	N–N	0	0.37
		20	SB	–	Unheated	N-HPC	0	3.11
		200	SB	–	Composite	N-HPC	0	2.7
		400	SB	–	Composite	N-HPC	0	1.8
		600	SB	–	Composite	N-HPC	0	1.21
		25	SB	–	Unheated	N-HPC	0	5.53
		200	SB	–	Composite	N-HPC	0	3.58
		400	SB	–	Composite	N-HPC	0	1.64
		600	SB	–	Composite	N-HPC	0	0.81
		25	SB	–	Unheated	N-HPC	0	4.29
		200	SB	–	Composite	N-HPC	0	3
		400	SB	–	Composite	N-HPC	0	1.83
		600	SB	–	Composite	N-HPC	0	0.81
		25	S	–	Unheated	N–N	0	0.93
		200	S	–	Composite	N–N	0	0.21
		400	S	–	Composite	N–N	0	0.14
		600	S	–	Composite	N–N	0	0.17
		25	S	–	Unheated	N-HPC	0	0.9
		200	S	–	Composite	N-HPC	0	0.23
		400	S	–	Composite	N-HPC	0	0.12
		600	S	–	Composite	N-HPC	0	0.07
		25	S	–	Unheated	N-HPC	0	1.19
		200	S	–	Composite	N-HPC	0	0.4
		400	S	–	Composite	N-HPC	0	0.13
		600	S	–	Composite	N-HPC	0	0.03
		25	S	–	Unheated	N–N	0	1.36
		200	S	–	Composite	N–N	0	0.48
		400	S	–	Composite	N–N	0	0.17
		600	S	–	Composite	N–N	0	0.17
Zalhaf et al. (2024)	Push-off test	25	C	–	Unheated	N–N	0	2.41
		200	C	–	Composite	N–N	0	2.28
		400	C	–	Composite	N–N	0	1.4
		600	C	–	Composite	N–N	0	1.14
		25	C	–	Unheated	N-HPC	1	3
		200	C	–	Composite	N-HPC	1	2.9
		400	C	–	Composite	N-HPC	1	2.62
		600	C	–	Composite	N-HPC	1	2.44
		25	C	–	Unheated	N-HPC	0	2.77
		600	C	–	Composite	N-HPC	0	1.36
		25	C	–	Unheated	N-HPC	0	2.88
		600	C	–	Composite	N-HPC	0	1.83
		25	C	–	Unheated	N-HPC	0.5	2.68
		600	C	–	Composite	N-HPC	0.5	2.06
		25	C	–	Composite	N-HPC	0.5	2.9
		600	C	–	Composite	N-HPC	0.5	1.03

Refs.	Type of test	*T*	SR	*α*	HP	CO	*F*	IBS
Shang et al. (2021)	Push-off test	20	SB	–	Unheated	N-HPC	2	1.87
		20	SB	–	Unheated	N-HPC	2	2.68
		20	SB	–	Unheated	N-HPC	2	1.61
		200	SB	–	Substrate	N-HPC	2	2.6
		200	SB	–	Substrate	N-HPC	2	2.26
		200	SB	–	Substrate	N-HPC	2	2.33
		400	SB	–	Substrate	N-HPC	2	2.66
		400	SB	–	Substrate	N-HPC	2	3.57
		400	SB	–	Substrate	N-HPC	2	3.52
		600	SB	–	Substrate	N-HPC	2	1.93
		600	SB	–	Substrate	N-HPC	2	2.53
		600	SB	–	Substrate	N-HPC	2	2.53
		600	WB	–	Substrate	N-HPC	2	1.59
		600	WB	–	Substrate	N-HPC	2	1.61
		600	WB	–	Substrate	N-HPC	2	1.68
		600	SB	–	Substrate	N-HPC	2	2.8
		600	SB	–	Substrate	N-HPC	2	3.4
		600	SB	–	Substrate	N-HPC	2	2.17
		600	SB	–	Substrate	N-HPC	2	2.54
		600	SB	–	Substrate	N-HPC	2	2.18
		600	SB	–	Substrate	N-HPC	2	2.16
		600	SB	–	Substrate	N-HPC	2	1.9
		600	SB	–	Substrate	N-HPC	2	1.73
		600	SB	–	Substrate	N-HPC	2	2.65
		600	SB	–	Substrate	N-HPC	2	1.32
Abo Sabah et al. (2019)	Tensile test	25	G	–	Unheated	N-HPC	6	6.95
		100	G	–	Composite	N-HPC	6	4.8
		200	G	–	Composite	N-HPC	6	3.3
		300	G	–	Composite	N-HPC	6	2.8
		400	G	–	Composite	N-HPC	6	2.1
		500	G	–	Composite	N-HPC	6	1.9
		25	SB	–	Unheated	N-HPC	6	8.53
		100	SB	–	Composite	N-HPC	6	6.2
		200	SB	–	Composite	N-HPC	6	5.8
		300	SB	–	Composite	N-HPC	6	4.3
		400	SB	–	Composite	N-HPC	6	3.6
		500	SB	–	Composite	N-HPC	6	2.1
Gao et al. (2019)	Tensile test	22	WB	–	Unheated	N–N	0	1.16
		22	WB	–	Unheated	N–N	0	0.93
		22	WB	–	Unheated	N–N	0	0.93
		200	WB	–	Composite	N–N	0	1.3
		200	WB	–	Composite	N–N	0	1.35
		200	WB	–	Composite	N–N	0	1.38
		400	WB	–	Composite	N–N	0	1.27
		400	WB	–	Composite	N–N	0	1.21
		400	WB	–	Composite	N–N	0	1
		600	WB	–	Composite	N–N	0	0
		800	WB	–	Composite	N–N	0	0
		22	WB	–	Unheated	N-HPC	1.7	2.35
		22	WB	–	Unheated	N-HPC	1.7	2.73
		22	WB	–	Unheated	N-HPC	1.7	2.12

Refs.	Type of test	*T*	SR	*α*	HP	CO	*F*	IBS
		200	WB	–	Composite	N-HPC	1.7	2.26
		200	WB	–	Composite	N-HPC	1.7	2.45
		200	WB	–	Composite	N-HPC	1.7	2.29
		400	WB	–	Composite	N-HPC	1.7	1.66
		400	WB	–	Composite	N-HPC	1.7	1.72
		400	WB	–	Composite	N-HPC	1.7	1.71
		600	WB	–	Composite	N-HPC	1.7	1.5
		600	WB	–	Composite	N-HPC	1.7	1.36
		600	WB	–	Composite	N-HPC	1.7	1.43
		800	WB	–	Composite	N-HPC	1.7	0.48
		800	WB	–	Composite	N-HPC	1.7	0
		800	WB	–	Composite	N-HPC	1.7	0.38
		22	WB	–	Unheated	N–N	0	2.12
		22	WB	–	Unheated	N–N	0	2.01
		22	WB	–	Unheated	N–N	0	2.04
		200	WB	–	Substrate	N–N	0	1.85
		200	WB	–	Substrate	N–N	0	2.42
		200	WB	–	Substrate	N–N	0	2.75
		400	WB	–	Substrate	N–N	0	1.76
		400	WB	–	Substrate	N–N	0	2.01
		400	WB	–	Substrate	N–N	0	1.98
		600	WB	–	Substrate	N–N	0	1.48
		600	WB	–	Substrate	N–N	0	1.7
		600	WB	–	Substrate	N–N	0	1.53
		22	WB	–	Unheated	N-HPC	1.7	1.94
		22	WB	–	Unheated	N-HPC	1.7	1.72
		22	WB	–	Unheated	N-HPC	1.7	2.22
		200	WB	–	Substrate	N-HPC	1.7	2.55
		200	WB	–	Substrate	N-HPC	1.7	2.84
		200	WB	–	Substrate	N-HPC	1.7	2.25
		400	WB	–	Substrate	N-HPC	1.7	2.05
		400	WB	–	Substrate	N-HPC	1.7	2.39
		400	WB	–	Substrate	N-HPC	1.7	2.46
		600	WB	–	Substrate	N-HPC	1.7	1.79
		600	WB	–	Substrate	N-HPC	1.7	2.01
		600	WB	–	Substrate	N-HPC	1.7	1.76
Ouyang et al. (2023)	Tensile test	20	SB	–	Unheated	N-HPC	1.6	1.99
		20	SB	–	Unheated	N-HPC	1.6	2.52
		300	SB	–	Substrate	N-HPC	1.6	1.59
		300	SB	–	Substrate	N-HPC	1.6	1.97
		500	SB	–	Substrate	N-HPC	1.6	1.82
		500	SB	–	Substrate	N-HPC	1.6	1.84
		300	SB	–	Substrate	N-HPC	1.6	2.15
		300	SB	–	Substrate	N-HPC	1.6	2.21
		500	SB	–	Substrate	N-HPC	1.6	1.77
		500	SB	–	Substrate	N-HPC	1.6	1.58

Acknowledgements
Not applicable.

Author contributions
NMZ: carried out the research plan, the artificial neural network analysis, the theoretical work, writing and reviewing the article.

Funding
Open access funding provided by The Science, Technology & Innovation Funding Authority (STDF) in cooperation with The Egyptian Knowledge Bank (EKB). Not applicable.

Availability of data and materials
The data and materials used to support the findings of this study are available from the corresponding author and can be obtained through e-mail communication with the author at Nagat.zalhaf@eng.kfs.edu.eg.

Declarations

Ethics approval and consent to participate
Not applicable.

Consent for publication
The author agrees that the article will be published after acceptance.

Informed consent
Not applicable.

Competing interests
The authors declare that they have no competing interests.

Received: 26 May 2024 Accepted: 28 November 2024

References

Abbas, H., Al-Salloum, Y. A., Elsanadedy, H. M., & Almusallam, T. H. (2019). ANN models for prediction of residual strength of HSC after exposure to elevated temperature. *Fire Safety Journal, 106*, 13–28. https://doi.org/10.1016/j.firesaf.2019.03.011

Abo Sabah, S. H., Zainal, N. L., Bunnori, N. M., Johari, M. A., & Hassan, M. H. (2019). Interfacial behavior between normal substrate and green ultra-high-performance fiber-reinforced concrete under elevated temperatures. *Structural Concrete, 20*(6), 1896–1908. https://doi.org/10.1002/suco.201900152

ACI 318. (2008). *Building code requirements for structural concrete (ACI 318–08) and commentary*. American Concrete Institute, PO Box 9094, Farmington Hills, MI 48333–9094, USA, 2008, 471 p.

Al Hamd, R. S., Alzabeebee, S., Cunningham, L. E., & Gales, J. (2022). Bond behaviour of rebar in concrete at elevated temperatures: A soft computing approach. *Fire and Materials, 47*, 804–814. https://doi.org/10.1002/fam.3123

Albidah, A., Abadel, A., Alrshoudi, F., Altheeb, A., & AbbasAl-Salloum, H. Y. (2020). Bond strength between concrete substrate and metakaolin geopolymer repair mortars at ambient and elevated temperatures. *Journal of Material Research Technology, 5*(9), 10732–10745. https://doi.org/10.1016/j.jmrt.2020.07.092

Albostami, A. S., Al Hamd, R. S., & Alzabeebee, S. (2023). Soft computing models for assessing bond performance of reinforcing bars in concrete at high temperatures. *Innovative Infrastructure Solutions, 8*, 218. https://doi.org/10.1007/s41062-023-01182-x

Babalola, O. E., Awoyera, P. O., Le, D. H., & Romero, L. B. (2021). A review of residual strength properties of normal and high strength concrete exposed to elevated temperatures: Impact of materials modification on behaviour of concrete composite. *Construction and Building Materials, 296*, 123448. https://doi.org/10.1016/j.conbuildmat.2021.123448

Behforouz, B., Tavakoli, D., Gharghani, M., & Ashour, A. (2023). Bond strength of the interface between concrete substrate and overlay concrete containing fly ash exposed to high temperature. *Structures, 49*, 183–197. https://doi.org/10.1016/j.istruc.2023.01.122

Cao, K., Li, H., Liu, G., Huang, Z., & Wu, G. (2023). Bonding properties between steel–basalt hybrid fibers reinforced cementitious composites and existing concrete at high temperatures. *Journal of Building Engineering, 70*, 106371. https://doi.org/10.1016/j.jobe.2023.106371

CEB-FIP Model Code, Comité Euro-International du Béton, Secretariat Permanent, Case Postale 88, CH-1015 Lausanne, Switzerland, 1990, 437 p.

Chen, H., Yang, J., & Chen, X. A. (2021). Convolution-based deep learning approach for estimating compressive strength of fiber reinforced concrete at elevated temperatures. *Construction and Building Materials, 313*, 125437. https://doi.org/10.1016/j.conbuildmat.2021.125437

Chen, Z., Xiao, J., Ding, T., & Liu, B. (2023). Push-off test on concrete–concrete interface with different types of concrete after elevated temperatures. *Construction and Building Materials, 377*, 131157. https://doi.org/10.1016/j.conbuildmat.2023.131157

Daneshvar, D., Behnood, A., & Robisson, A. (2022). Interfacial bond in concrete-to-concrete composites: A review. *Construction and Building Materials, 359*, 129195. https://doi.org/10.1016/j.conbuildmat.2022.129195

Elsanadedy, H. M., Abbas, H., Al-Salloum, Y. A., & Almusallam, T. H. (2014). Prediction of intermediate crack debonding strain of externally bonded FRP laminates in RC beams and one-way slabs. *Journal of Composite for Construction*. https://doi.org/10.1061/(ASCE)CC.1943-5614.0000462

Elsanadedy, H. M., Abbas, H., Al-Salloum, Y. A., & Almusallam, T. H. (2016). Shear strength prediction of HSC slender beams without web reinforcement. *Materials and Structures, 49*(9), 3749–3772. https://doi.org/10.1617/s11527-015-0752-x

Elsanadedy, H. M., Al-Salloum, Y. A., Abbas, H., & Alsayed, S. H. (2012). Prediction of strength parameters of FRP confined concrete. *Composites Part B: Engineering, 43*, 228–239. https://doi.org/10.1016/j.compositesb.2011.08.043

Eurocode 2. (2004). *Design of concrete structures—Part 1–1: General rules and rules for buildings*. European Committee for Standardization, Avenue Marnix 17, B-1000 Brussels, Belgium, 225 p. (with corrigendum dated of 16 January 2008)

Farhangi, V., Moradi, M. J., Daneshvar, K., & Hajiloo, H. (2024). Application of artificial intelligence in predicting the residual mechanical properties of fiber reinforced concrete (FRC) after high temperatures. *Construction and Building Materials, 411*, 134609. https://doi.org/10.1016/j.conbuildmat.2023.134609

Farouk, A. I., & Jinsong, Z. (2022). Prediction of Interface Bond Strength Between Ultra-High-Performance Concrete (UHPC) and Normal Strength Concrete (NSC) Using a Machine Learning Approach. *Arabian Journal for Science and Engineer, 47*, 5337–5363. https://doi.org/10.1007/s13369-021-06433-6

Gao, S., Zhao, X., Qiao, J., Guo, Y., & Hu, G. (2019). Study on the bonding properties of Engineered Cementitious Composites (ECC) and existing concrete exposed to high temperature. *Construction and Building Materials, 196*, 330–344. https://doi.org/10.1016/j.conbuildmat.2018.11.136

Gao, W., Hu, K., Dai, J., Dong, K., Yu, K., & Fang, L. (2018). Repair of fire-damaged RC slabs with basalt fabric-reinforced shotcrete. *Construction and Building Materials, 185*, 79–92. https://doi.org/10.1016/j.conbuildmat.2018.07.043

Garson, D. G. (1991). Interpreting neural network connection weights. *AI Expert, 6*(4), 46–51.

Ghazy, M. F., Abd Elaty, M. A., & Zalhaf, N. M. (2021). Prediction of temperature distribution and fire resistance of RC slab using artificial neural networks. *Int. J. Structural Engineering, 11*(1), 1–18. https://doi.org/10.1504/IJSTRUCTE.2021.112084

Ghazy, M. F., Abd Elaty, M. A., & Zalhaf, N. M. (2022). Mechanical properties of HPC incorporating fly ash and ground granulated blast furnace slag after exposure to high temperatures. *Periodica Polytechnica Civil Engineering, 66*(3), 761–774. https://doi.org/10.3311/PPci.19751

Ghazy, M. F., Abd Elaty, M. A., & Zalhaf, N. M. (2023). Performance of normal strength concrete slab strengthened with high-performance concrete after exposure to elevated temperature. *Fire Technology*. https://doi.org/10.1007/s10694-023-01439-y

Gohnert, M. (2003). Horizontal shear transfer across a roughened surface. *Cement Concrete Compoite, 25*, 379–385. https://doi.org/10.1016/S0958-9465(02)00050-1

Guo, J. J., Song, Y. P., & Zhang, L. S. (2004). On shear behavior of new–old concrete bonding after exposure to high temperatures. *Engineering Mechanics, 21*(4), 133–138.
Haddad, R. H., Al-Mekhlafy, N., & Ashteyat, A. M. (2011). Repair of heat-damaged reinforced concrete slabs using fibrous composite materials. *Construction and Building Materials, 25*(3), 1213–1221. https://doi.org/10.1016/j.conbuildmat.2010.09.033
Hagan, M. T., & Menhaj, M. B. (1994). Training feedforward networks with the Marquardt algorithm. *IEEE Trans. Neural Network, 5*(6), 989–993. https://doi.org/10.1109/72.329697
Haido, J. H., Tayeh, B. A., Majeed, S. S., & Karpuzcu, M. (2021). Effect of high temperature on the mechanical properties of basalt fibre self-compacting concrete as an overlay material. *Construction and Building Materials, 268*, 121725. https://doi.org/10.1016/j.conbuildmat.2020.121725
Jie, S. (2007). *The Study on Bonding Behaviors of Reactive Powder Concrete and Ordinary concrete*. Master's Degree Thesis, Beijing Jiaotong University, Beijing, China.
Kowalski, C. J. (1972). On the effects of non-normality on the distribution of the sample product-moment correlation coefficient. *Journal of the Royal Statistical Society. Series C (Applied Statistics), 21*(1), 1–12. https://doi.org/10.2307/2346598
Ma, Q., Guo, R., Zhao, Z., Lin, Z., & He, K. (2015). Mechanical properties of concrete at high temperature—a review. *Construction and Building Materials, 93*, 371–383. https://doi.org/10.1016/j.conbuildmat.2015.05.131
Mansour, W., & Fayed, S. (2021a). Flexural rigidity and ductility of RC beams reinforced with steel and recycled plastic fibers. *Steel Composite Structure, 41*(3), 317–334. https://doi.org/10.12989/SCS.2021.41.3.317
Mansour, W., & Fayed, S. (2021b). Effect of interfacial surface preparation technique on bond characteristics of both NSC-UHPFRC and NSC-NSC composites. *Structures, 29*, 147–166. https://doi.org/10.1016/j.istruc.2020.11.010
Momayez, A., Ehsani, M. R., Ramezanianpour, A. A., & Rajaie, H. (2005). Comparison of methods for evaluating bond strength between concrete substrate and repair materials. *Cement Concrete Research, 35*, 748–757. https://doi.org/10.1016/j.cemconres.2004.05.027
Moradi, M., Khaleghi, M., Salimi, J., Farhangi, V., & Ramezanianpour, A. (2021). Predicting the compressive strength of concrete containing metakaolin with different properties using ANN. *Measurement, 183*, 109790. https://doi.org/10.1016/j.measurement.2021.109790
Naser, M., Abu-Lebdeh, G., & Hawileh, R. (2012). Analysis of RC T-beams strengthened with CFRP plates under fire loading using ANN. *Construction and Building Materials, 37*(10), 301–309. https://doi.org/10.1016/j.conbuildmat.2012.07.001
Nazemi, E., Roshani, G., Feghhi, S., Setayeshi, S., Zadeh, E. E., & Fatehi, A. (2016). Optimization of a method for identifying the flow regime and measuring void reaction in a broad beam gamma-ray attenuation technique. *International Journal of Hydrogen Energy, 41*(18), 7438–7444. https://doi.org/10.1016/J.IJHYDENE.2015.12.098
Ouyang, J., Guo, G., Wang, X., Fu, C., Wan, F., & Pan, T. (2023). Effects of interface agent and cooling methods on the interfacial bonding performance of engineered cementitious composites (ECC) and existing concrete exposed to high temperature. *Construction and Building Materials, 376*, 131054. https://doi.org/10.1016/j.conbuildmat.2023.131054
Randl, N (1997) *Investigations on transfer of forces between old and new concrete at different joint roughness*. PhD thesis, University of Innsbruck, 379 p. (in German)
Santos, M. D., & Júlio, E. N. B. S. (2014). Interface Shear Transfer on Composite Concrete Members. *ACI Structural Journal, 111*, 113–121. https://doi.org/10.14359/51686543
Santos, P. M., & Julio, E. N. (2007). Correlation between concrete-to-concrete bond strength and the roughness of the substrate surface. *Materials, 21*, 1688–1695. https://doi.org/10.1016/j.conbuildmat.2006.05.044
Santos, P.M.D., & Júlio, E.N.B.S. (2010). Recommended improvements to current shear friction provisions of model code. In: 3rd Fib International Congress, Washington, DC, May 29-June 02.
Shafighfard, T., Bagherzadeh, F., Rizi, R. A., & Yoo, D. Y. (2022). Data-driven compressive strength prediction of steel fiber reinforced concrete (SFRC) subjected to elevated temperatures using stacked machine learning algorithms. *Journal of Material Research Technology, 21*, 3777–3794. https://doi.org/10.1016/j.jmrt.2022.10.153
Shang, X. Y., Xu, F. Z., Yu, J. T., Li, L. Z., & Lu, Z. D. (2021). Study on the interfacial shear performance between engineered cementitious composites and concrete after being subjected to high temperatures. *Journal of Building Engineer, 44*, 103328. https://doi.org/10.1016/j.jobe.2021.103328
Sun, J., Fan, J., Chen, A., & Yuan, L. (2022). Interfacial properties between autoclaved aerated concrete and concrete after high temperature. *Journal of Building Engineering, 60*, 105213. https://doi.org/10.1016/j.jobe.2022.105213
Varona, F. B., Baeza, F. J., Bru, D., & Ivorra, S. (2018). Evolution of the bond strength between reinforcing steel and fibre reinforced concrete after high temperature exposure. *Construction and Building Materials, 176*, 359–370. https://doi.org/10.1016/j.conbuildmat.2018.05.065
Wang, B., Li, Q., Liu, F., Wang, J., & Xu, S. (2018). Shear bond assessment of UHTCC repair using push-out test. *Construction and Building Materials, 164*, 206–216. https://doi.org/10.1016/j.conbuildmat.2017.12.148
Yehia, S. A., Fayed, S., Zakaria, M. H., & Shahin, R. I. (2024). Prediction of RC T-Beams Shear Strength Based on Machine Learning. *International Journal of Concrete Structures and Materials, 18*, 52. https://doi.org/10.1186/s40069-024-00690-z
Zalhaf, N. M., Fayed, S., & Zakaria, M. H. (2024). Interfacial shear behavior of composite concrete substrate to high performance concrete overly after exposure to elevated temperature. *International Journal of Concrete Structures and Materials*. https://doi.org/10.1186/s40069-023-00654-9

Publisher's Note

Nagat M. Zalhaf is assistant professor in the department of Civil Engineering, Faculty of Engineering, Kafrelsheikh University, Kafrelsheikh city, Egypt.